J 2022

FACULDADE DE ENGENHARIA
UNIVERSIDADE DO PORTO

INFLUENCE OF WINDINGS DESIGN ON THE THERMAL PERFORMANCE OF CORE-TYPE POWER TRANSFORMERS USING MINERAL OIL AND NATURAL ESTER AS COOLING FLUID

DIOGO PEREIRA GONÇALVES
MASTER THESIS IN CHEMICAL ENGINEERING
PRESENTED TO THE FACULTY OF ENGINEERING
OF THE UNIVERSITY OF PORTO

Master in Chemical Engineering

INFLUENCE OF WINDINGS DESIGN ON THE THERMAL PERFORMANCE OF CORE-TYPE POWER TRANSFORMERS USING MINERAL OIL AND NATURAL ESTER AS COOLING FLUID

Master dissertation

of

Diogo Pereira Gonçalves

Developed within the course of dissertation

held in

Efacec Energia, Máquinas e Equipamentos Elétricos, S.A.
R&D Department of Transformers Unit

Supervisor at FEUP: **Dr.ª Soraia Ferreira Neves**

Joint supervisor(s) at FEUP: **Dr.ª Mónica Filgueiras**

Coordinator at EFACEC: **Eng.ª Sandra Couto**

“I know I was born, and I know that I´ll die, the in-between is mine, I am mine”

Edward Louis Severson III

Acknowledgment

First of all, I would like to thank Efacec for giving me this incredible opportunity to do my Master dissertation in such a prestigious company, which gave me the best conditions for the realization of the work, and whose environment was very positive during the last 4 and a half months.

I want to thank Soraia Ferreira Neves and Mónica Cristina Ferreira da Silva Filgueiras, supervisors of this dissertation are integrated members of CEFT – Transport Phenomena Research Center, financially supported by LA/P/0045/2020 (ALiCE), UIDB/00532/2020 and UIDP/00532/2020 (CEFT), funded by national funds through FCT/MCTES (PIDDAC), for all the support and guidance given throughout this period. You helped me to evolve academically and personally, with all the teachings given, all the questions answered, the ways of looking at problems and knowing how to approach them and allowed me to do the proposed work in the most correct way possible, which by myself, I could not do. I will never forget the importance you had in building the engineer I will become. Wish all the best for you both.

Thank you, Sandra Couto, for all the guidance, for being tireless throughout all the work that was done. For always being available to help me and clear up all the questions, no matter how silly they were. For having welcomed me in the best way I could wish for in the world of industry and for helping to make me a future engineer capable of dealing with the problems of the world of work better than I would ever be able to.

Thank you, Rita, for being my pillar for the last 7 years, for continuing to be, and for being my life partner, now and forever.

A special thanks to my father Paulino, my mother Susana, my brother Pedro, and my grandmother Susana. This achievement is for you, if I am what I am today it is because of you, and no written thanks can describe the importance you have had in the 23 years of my existence and in all my academic journey.

Thank you to all my family for always being there for me.

Thank you to the Djiamantjizinhos of M&A, for making this journey, the best I could have wished for my college years. We went in as amiguinhos, we came out as Engineers and true limões.

To all the Efacec Transformers R&D Thermal and Fluids team, thank you for receiving me in such a warm way and allowed me to feel part of the team. A special thanks to Ricardo Castro Lopes, for all the teachings given in the area of transformers, an area that I never thought would be part of my dissertation topic, but that I can now understand much better thanks to all the help given and questions clarified. Thanks also to Catarina Sousa for all the help in the CFD, all the headaches you helped me to solve, and I take this opportunity to apologize if I was annoying all the times I asked for access to the workstation.

Thank you, Gabriel, for being my working partner, for living with me this transition and the embracing of such a challenging project for both of us. I wish you great success in the rest of your academic and professional life. We will see each other around.

To all the members of CEFT, namely the E102 group, who made my workdays much more cheerful, and helped me to face the day-to-day problems in a much better mood. It was amazing to feel a little bit a part of this group especially over the last 2 months.

Thank you to all the other people who have made the last 5 years unforgettable, who have taught me, and who I have had the opportunity to teach. I'm sure we will continue to see each other around.

Abstract

Power transformers (PT), are devices used worldwide in the electrical energy transmission and distribution systems, being essential for high transmission voltages transformation into lower voltages for both domestic and industrial usage. Being the target of several studies to improve their performance, one of the subjects of interest among the community is the internal cooling of PTs, because excessive heat inside the transformer leads to high temperatures which contribute to the degradation of its insulating materials. This degradation can result in reduction of the transformer life-time and ultimately in fatal failure. Internal cooling (concerning the cooling phenomenon occurring inside the PT tank with particular importance in its windings) is performed by a cooling fluid that travels through the windings' channels, cooling the discs (heat source). The objective of this work was to study the influence that the design of the windings of a core type PT plays in its internal cooling when this is performed by mineral oil and natural ester, and also to develop a machine learning model capable to predict the thermal behavior of the winding.

Steady-state Computational Fluid Dynamics (CFD) simulations were performed, considering a 2D axisymmetric model (after validation with a 3D axisymmetric model and with experimental results) of a core-type PT winding. Three values were defined for axial channel width, radial channel height, and Reynolds number at the winding entrance. A machine learning tool was also used to obtain correlations between the PT design parameters and the results obtained in the simulations.

54 hydraulic simulations (without considering heat transfer) were performed to obtain the pressure drop inside windings, considering a combination of different geometrical features and different fluids. Other 54 simulations were performed considering the heat transfer phenomena, to obtain the values of 6 thermal parameters of interest (top-oil, average-oil, average-winding and hot-spot temperatures, hot-spot factor and Nusselt number) to observe the influence of varying geometric characteristics of the winding and the use of two different fluids on the results of these parameters. The results obtained were used to train a machine learning algorithm, aiming to build a tool capable of predicting the thermal parameters of interest, for a given design.

In terms of hydraulics, the results obtained show that for the existence of heat transfer, the pressure drop trend along the flow is similar to when does not exist heat transfer. Regarding the thermal properties it was observed that the variation of the Reynolds number at the inlet is the parameter that most affects the temperature distribution inside the winding. The geometric parameter that most influences the results is the width of the axial channels.

Furthermore, the natural ester showed the best cooling performance, however it also implies higher pressure drops.

The machine learning tool showed to be highly promising in predicting the thermal performance of a core type PT, however it needs to be improved (by feeding it with more data) to ensure a wider and more accurate use.

Keywords: core type power transformers, CFD, machine learning, windings, internal cooling, mineral oil, natural ester, heat transfer, flow, numerical simulation

Resumo

Os transformadores de potência (PT), são aparelhos utilizados a uma escala global, nas redes de transporte e distribuição de energia elétrica, essenciais para conversão de alta-tensão numa tensão compatível com utilização industrial e doméstica. Sendo alvo de diversos estudos para melhorar o seu desempenho, uma das matérias que suscita bastante interesse entre a comunidade é o arrefecimento interno dos PT, pois o calor excessivo no interior do transformador resulta em temperaturas elevadas levando à degradação dos seus materiais isolantes. Esta degradação pode resultar na diminuição do tempo de vida do transformador e, em última instância, numa falha fatal. O arrefecimento interno (que diz respeito ao arrefecimento no interior da cuba, com particular importância nos enrolamentos), é efetuado por um fluido que percorre os canais do enrolamento, arrefecendo os discos (fonte de calor). O objetivo deste trabalho foi estudar a influência que a geometria dos enrolamentos de um PT tipo core desempenha no seu arrefecimento interno, quando este é realizado por óleo mineral e ester natural, e também desenvolver um modelo de *machine learning* capaz de prever o desempenho térmico do enrolamento.

Foram realizadas simulações de CFD em estado estacionário, considerando um modelo 2D axissimétrico (após validação com um modelo 3D axissimétrico e com resultados experimentais) de um enrolamento de um PT tipo Core. Definiram-se 3 valores de largura dos canais axiais, de altura dos canais radiais e de número de Reynolds à entrada do enrolamento. Utilizou-se uma ferramenta de *machine learning,* visando obter correlações entre os parâmetros de design do PT e os resultados obtidos nas simulações.

Inicialmente realizaram-se 54 simulações de hidráulica (sem considerar transferência de calor) para obter os valores de perda de carga ao longo do enrolamento para diferentes configurações geométricas e fluidos. Outras 54 simulações foram realizadas, considerando o transporte de calor, para obter os valores de 6 parâmetros térmicos de interesse (temperaturas do óleo superior, médio, temperatura média do enrolamento e do seu ponto mais quente, fator de ponto quente e número de Nusselt) para se observar a influência da variação das características geométricas do enrolamento e da utilização dos dois diferentes fluidos nos resultados destes parâmetros. Alimentaram-se os resultados obtidos a um algoritmo de *machine learning,* visando a construção de uma ferramenta capaz de prever os resultados térmicos de interesse, para determinado design.

A nível da hidráulica, os resultados obtidos demonstram que a existência de transferência de calor mantém a tendência de perda de carga ao longo do enrolamento. Relativamente às propriedades térmicas observou-se que a variação do número de Reynolds, à entrada, é o parâmetro que mais afeta a distribuição de temperaturas no enrolamento, e o parâmetro geométrico que mais influencia os resultados é a largura dos canais axiais. Concluiuse ainda que o ester natural arrefece melhor os discos, contudo apresenta elevadas perdas de carga no escoamento.

A ferramenta de *machine learning* mostrou ser promissora na previsão do desempenho térmico de um PT tipo core, no entanto necessita de aperfeiçoamento (alimentada com mais dados) para garantir uma utilização mais ampla e precisa.

Palavras Chave: Transformadores de potência tipo core, CFD, *machine learning*, enrolamentos, arrefecimento interno, óleo mineral, ester natural, transferência de calor, escoamento, simulação numérica

Declaration

I hereby declare, under word of honour, that this work is original and that all non-original contributions is indicated and due reference is given to the author and source

04/07/2022

Diogo Gonçalves

Index

List of Figures

List of Tables

Notation and Glossary

A	Area	m^2
C_p	Specific heat	$J\ kg^{-1}\ K^{-1}$
k	Thermal conductivity	$W\ m^{-1}\ K^{-1}$
L	Length	m
$\dot{m}$	Mass flow-rate	$kg\ h^{-1}$
Q	Heat	J
D_h	Hydraulic diameter	m
T	Temperature	ºC
v	Velocity	$m\ s^{-1}$
Re	Reynolds number	
r	Radius	m
Nu	Nusselt number	
h	Convective coefficient	$W\ m^{-2}\ K^{-1}$
P	Pressure	Pa
Δt	Time step	s
Δh	Distance	m

Greek Letters

ρ		$kg\ m^{-3}$
μ		$Kg\ m^{-1}\ s^{-1}$

Indexes

hot-spot	Hot-spot
top-oil	Top-oil
average-winding	Average-winding
bottom-oil	Bottom-oil
Disc	Disc
washer	Washer
axial	Axial channel
radial	Radial channel
In	Inlet
fluid	Fluid
out	Outlet
c	Channel
max	maximum
i	Index or counter

List of Acronyms

EFME	Empresa Fabril de Máquina Elétricas
ACEC	Ateliers de Constructions Életriques de Charleroi
R&D	Research and Development
CFD	Computational Fluid Dynamics
AC	Alternate Current
DC	Direct current
ML	Machine Learning
ON	Oil with natural convection
OD	Oil with directed convection
HSF	Hot-spot factor
PT	Power transformer
3D	Three dimensions
2D	Two dimensions
UDF	User defined function

1 Introduction

1.1 Framing and presentation of the work

Power transformers are devices created in the mid-19th century. Since that time, they have played a key role in power distribution worldwide, and their fundamental principle is the use of electromagnetic induction to increase or decrease the voltage of alternating current. The electromagnetic induction is generated in the magnetic core of power transformers, which when energized, create a magnetic flux that causes the high voltage winding to transfer current to the low voltage winding (to decrease the voltage) or vice versa (to increase the voltage; [1,2]). Figure 1 shows an experimental set-up of a core-type power transformer.

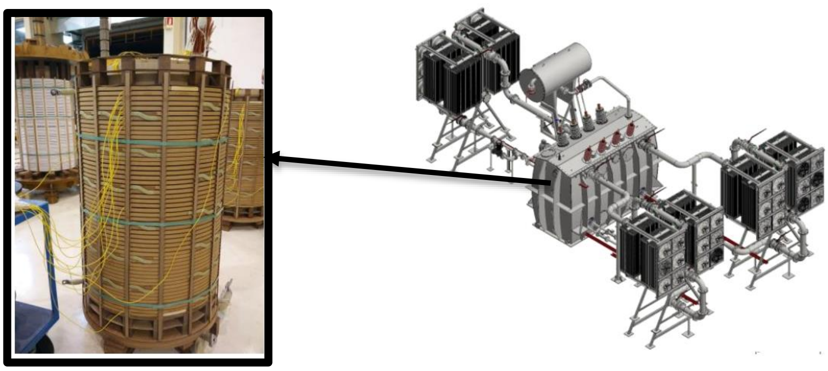

Figure 1 - Efacec's experimental set-up: 15 MVA core-type power transformer and the location of their windings (inside the tank)

Given their wide application, power transformers are the target of several studies to improve their performance. One of the topics of interest is the internal cooling of transformers, which occurs in their windings. The windings are made up of copper discs, which produce energy, releasing heat, and to avoid the deterioration of the materials that compose them, a cooling fluid is used to prevent the temperature from increasing drastically [2]. The cooling efficiency will be influenced by several factors, from the geometry of the winding channels to the cooling fluid circulation velocity.

This thesis will study how each of these factors influences the internal cooling of a core-type power transformer.

1.2 Presentation of the company

Efacec is a Portuguese group of companies that operate in the energy, engineering, environment, transports, and electric mobility fields, with a strong exporting profile, and is present in more than 65 countries. Efacec´s origin dates to 1905 with the foundation of the Mechanical Sawmill Society “A Moderna”. Further, in 1948, it was constituted EFME – *Empresa*

Fabril de Máquinas Eléctricas, SARL, that later, in 1962, grouped together with ACEC - *Ateliers de Constructions Électriques de Charleroi*, creating Efacec. By the year 2014, the company name changed to Efacec Power Solutions, SA (EPS) [3].

Nowadays, Efacec is one of the largest Portuguese industrial enterprises and a prestigious brand known worldwide in three main areas: Energy, Mobility and Environment [3].

1.3 Contribution of the author to the work

The application of esters in the internal cooling of core type power transformers is a subject that is being increasingly studied worldwide. Efacec Transformers R&D Thermal and Fluids team is performing an active part in the research on the theme. This thesis arises on a particular part of the overall research that focus on how the thermal behavior inside the windings of a core-type power transformer varies when using two distinct fluids for its internal cooling, given different geometric parameters. For this purpose, a winding geometry was built, the simulations were automated, and after obtaining the numerical results, a machine learning (ML) tool was created from scratch, to predict the thermal behavior of a winding when a set of input conditions are defined, for a given fluid (mineral oil and natural ester). The use of ML in the prediction of the results, plays a very important part on the study, as it appears as a new and expedite method to predict the better conditions to guarantee a more efficient cooling depending on the used cooling fluid.

1.4 Organization of the dissertation

This dissertation is divided in 6 main chapters and respective subchapters.

The Chapter 1 introduces the theme and scope of the dissertation, as well as the contribution to the work.

Chapter 2 provides a look into the state of the art of the transformers' operation, their internal cooling process, and the numerical methods and tools that can be used during the research and development of core-type power transformers.

Chapter 3 describes the materials and the methods taken into account for the execution of the work, all the considerations made and why were they made.

Chapter 4 presents all the results of the simulations made and the machine learning processes, and the respective discussion.

Chapter 5 consists of the conclusions obtained in this work.

Chapter 6 focus on the achievements made along the execution of the dissertation, as well as the future work that can be done, complementary to this study.

2 Context and state of the art

2.1 Power Transformers

With the invention of electromagnetic induction, in 1831, Michael Faraday introduced the principles that led to the creation of the first transformer and power distribution systems. However, the first transformer was only executed during the 1880s by three Hungarian engineers Károly Zipernowsky, Miksa Déri, and Ottó Bláthy, also responsible for the creation of the first transformer system with parallel distribution [4].

Transformers are used to increase or decrease the voltage in an alternate current (AC) electrical circuit. The use of DC (direct current) power presented issues due to its long-distance transmission. For instance, for a low voltage, it was necessary a very thick wire, which would be unpractical, and for high voltage, the wire would be thin but highly dangerous. With AC power, and by using power transformers, it was possible to change the voltage as convenient, along all the distribution grid, from the electrical energy generation location to our houses [1].

Essentially, a transformer consists of a static electrical device used in the transmission of electrical energy, through electromagnetic induction, between circuits within a power system. These power systems include a large network comprising serious generation locations, distribution points and connections, inside the system itself, or with systems around such as neighbor public services [2]. There are several types of transformers for different usages, made for higher or lower voltages, but in this work, particularly, will be considered core-type power transformers.

Power transformers are usually rated based on the power output they can continuously provide, at a specified frequency and voltage, under “usual” working conditions without overrunning the internal pre-defined temperature limitations [2,5]. As the power transformers’ insulation deteriorates with increasing temperatures, it should be selected considering its expected use time, limiting the operating temperature. The power rating refers to transformers’ continuous loading, representing a reference value for guarantees and tests concerning load losses and temperature rises [6]. The rating of a transformer is defined by the temperature tolerable by the insulation, and transformers are rated in Volts times Amperes, “VA”, with “kVA” and “MVA” meaning 1000 kVA and 10^6 kVA, respectively [5].

Transformers are made of various elements. In Figure 2, it is possible to see a scheme of the positioning of the main parts of a power transformer.

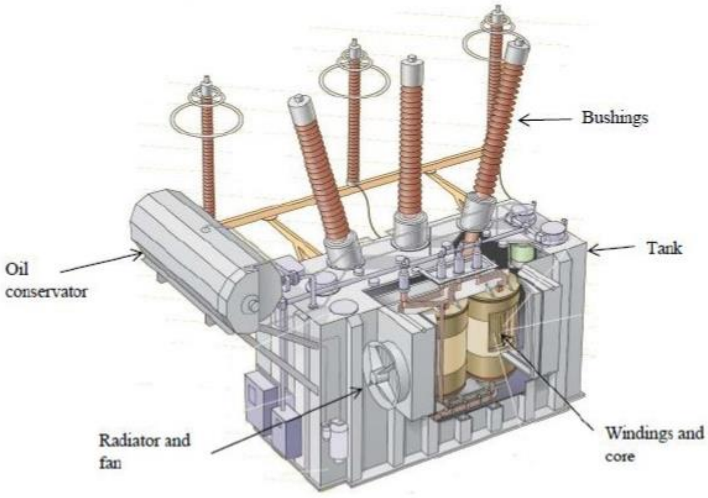

Figure 2 - Power transformer (adapted from [7]*)*

2.2 Power Transformers' Components

The key parts of a power transformer are the magnetic core, the windings and the tank, but besides these, there are several other important components and features such as the insulating materials, bushings and the external cooling system [8,9].

2.2.1 Magnetic core

The magnetic core represents an important part of a transformer, supporting the windings, providing low magnetic resistance to the magnetic flux, and reducing hysteresis loss. For that, the core is made of a set of steel sheets, with very low thickness, stacked on each other forming the core. The smaller the diameter of the core, the lower the iron losses, but the copper losses in the windings increase [9,10]. Figure 3 shows magnetic cores.

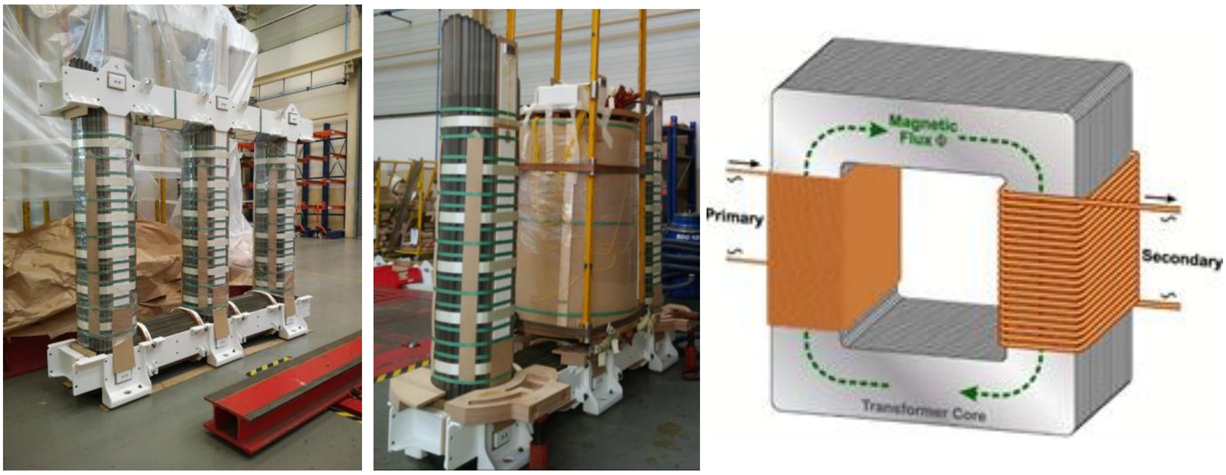

a) b)

Figure 3 - a) Magnetic core structure and one of the phases mounted in the central leg of the magnetic core (from an experimental setup transformer, courtesy of Efacec) ; b) transformer's magnetic core with primary and secondary windings (adapted from [11]*)*

2.2.2 Windings

The windings are the fundamental component of a transformer as they make the phenomenon of electromagnetic induction possible. Power transformers have primary and secondary windings, as their purpose is to change the voltage according to the user's need [2]. Assuming that the primary winding represents the input and the secondary winding the output, if it is intended to increase the voltage, the primary winding must have fewer turns than the secondary winding. This happens because, with the increase of turns around the core, there is the increase of the voltage and the decrease of the current. So, in the other way, if it is intended to decrease the voltage, the primary winding must have more turns than the secondary winding. When the voltage is increased, the transformer represents a step-up transformer, whereas, when the voltage is decreased, the transformer represents a step-down transformer [12,13]. Windings can be made by copper or aluminum, as they are both good conductors, what decreases the electrical losses, and copper is usually used in larger power transformers, while aluminum is more used in smaller power transformers [2,10]. Around and inside the windings there are insulating materials.

Based on the winding designs and technologies, there are two main types of power transformers: core-type and shell-type transformers. Once the electromagnetic principles are the same, the most noticeable difference between them concerns their construction. In the core-type transformers, the windings are located around the magnetic core, and in the shell-type transformers the magnetic core is located around the windings. Figure 4 represents the mechanical structure of the core and shell type transformers.

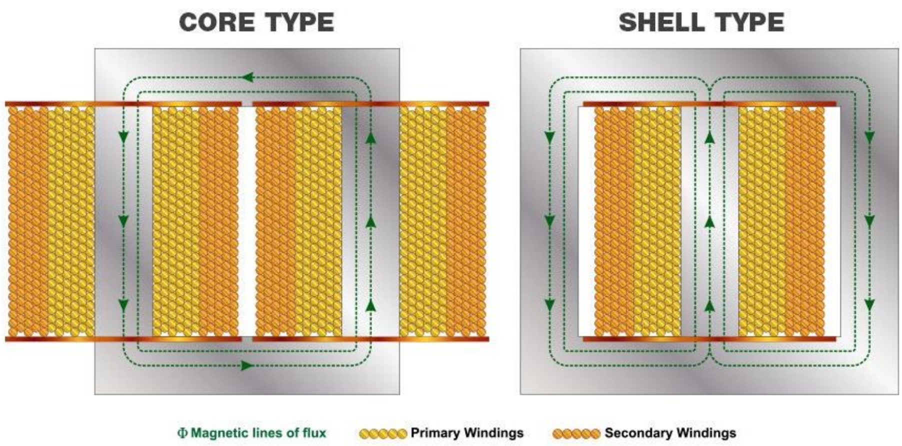

Figure 4 - Core type and Shell type transformers (adapted from [14]*)*

2.2.3 Insulating material

As the windings of a transformer operate at high voltages, it is important to provide electrical insulation in the regions with different voltages (e.g. between the windings and the core, other structural elements, and the tank) [12]. The insulation materials must have a series of properties, such as, dielectric strength and ability to withstand high temperatures. The materials commonly used are mineral oil, paper and other cellulosic materials such as pressboards, as they present a very high insulation capability [8]. Pressboard is also used to strengthen the electrical insulation and to provide dielectric distance between windings [9,12].

Insulation failures cause transformers' damage, and the insulation materials, namely the solid ones, are impossible to repair or replace, so transformers are very dependent on their performance. The aging of these materials affects their properties, being so, the transformers' lifetime is dependent on the lifetime of insulation materials [9].

The insulation in a transformer must be capable to withstand higher voltages than the normal operating ones due to a possible lightning strike or a short circuit in some part of the electrical system, which suddenly increases the voltage. So, the insulation should control this increase, to avoid damage of the system [12].

2.2.4 Bushings

Bushings are a connection terminal between the windings and the incoming or outgoing cables. They represent a secure passage of current, and work also as an insulator between the terminals and the tank.

2.3 Cooling system

Transformers are very efficient devices (about 99.5%), but they are not perfect. There are energy losses, especially in the windings, being the lost energy converted into heat. The increase of temperature inside the transformer, leads to deterioration of insulating material. Therefore, the transformers' cooling system represents an essential feature within the projection of the transformers, being composed by internal and external cooling [2]. Internal cooling refers to the cooling inside the tank (Figure 2), performed with cooling fluid, while external cooling is performed outside the tank (e.g., radiator and fan in Figure 2).

The cooling fluid works both as an electrical insulator and heat removal medium, and as the windings represent the biggest heat source, it is needed to have the fluid circulating inside passages near that heat source. The fluid circulates inside the tank, being heated up since the moment it enters in the tank, until its exit, where it is cooled in any external cooling system [2].

The circulation of the fluid, inside the tank, can be natural or forced. In natural circulation, the cooling fluid flows due to buoyancy forces, while if pumps are used, the flow of the cooling fluid will be forced or directed to the windings, and in those cases it is said that the convection is forced [2].

Based on the cooling medium and mechanism, it is possible to classify the type of transformer with a letter code composed by 4 letters (Table 1; [2]).

Table 1 - Cooling class letter description (adapted from [2]*)*

		Code Letter	Description
Internal	First Letter (Cooling medium)	O	Liquid with flash point less than or equal to 300ºC
		K	Liquid with flash point greater than 300ºC
		L	Liquid with no measurable flash point
	Second Letter (Cooling mechanism)	N	Natural convection through cooling equipment and windings
		F	Forced circulation through cooling equipment, natural convection in windings
		D	Forced circulation through cooling equipment, directed flow in man windings
External	Third letter (Cooling medium)	A	Air
		W	Water
	Fourth letter (Cooling medium)	N	Natural convection
		F	Forced circulation

In Figure 5 is shown the thermal diagram inside the transformer's windings as considered by IEC 60076-2 standard [15].

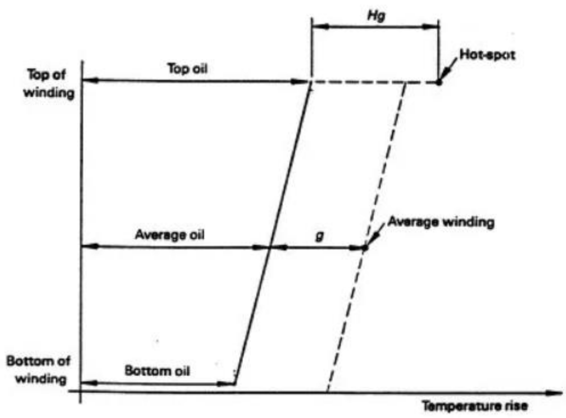

Figure 5 - Thermal model inside a transformer [15]

This model assumes that the temperature rise (winding-to-ambient or oil-to-ambient) varies linearly along the winding, from bottom to top. The left oblique line corresponds to oil temperature rise variation along the winding, while the right oblique line corresponds to the conductor temperature rise variation along the winding. According to this model, the temperature difference between the conductor and oil (winding-to-oil gradient, g) is considered constant along the winding. The diagram also represents the hot-spot rise (higher temperature rise in the winding) and the hot-spot factor (H), which informs how much the hot-spot gradient deviates from the constant (or average) gradient [16].

The hot-spot factor, HSF ("H" in Figure 5), can be obtained by applying experimentally obtained values (from temperature rise tests performed in power transformers) in Equation 1 [15,16].

$$HSF = \frac{(T_{hot-spot} - T_{top-oil})}{\left(T_{average\ winding} - \frac{(T_{top-oil} + T_{bottom-oil})}{2}\right)} \quad (1)$$

In a power transformer, the hot-spot winding temperature determines the harshest thermal aging rate of the solid insulating material (paper), so this temperature is a subject of interest among the community [17,18].

2.3.1 Insulating fluids

Different fluids are therefore used as insulators and coolants in transformers, and for this project the focus will be on mineral oil and esters. For a clearer idea of the chronology development and application of the different fluids, Figure 6 represents the development of insulating fluids in transformers' industry over the years [19].

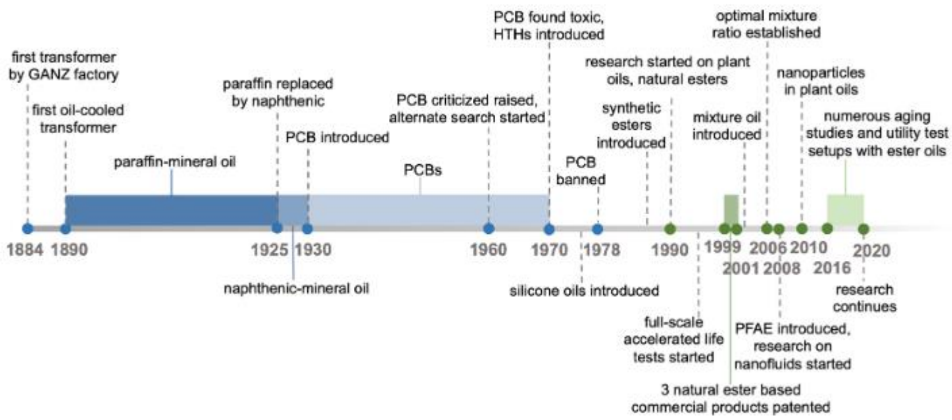

Figure 6 - Timeline development of insulating fluids in transformers industry [19]

One of the most widely used insulating liquids is mineral oil [2] essentially due to its excellent thermal insulation properties [20].

Mineral oil comes from the refining of crude oil. There are several types of mineral oils, and their use depends on the transformer type and its operating conditions, but it is important to note that their relevance is always based on electrical insulation and heat transfer rates in the windings and inside the tank [20,21]. However, as time went by, there were some worries being addressed about its lack of fire safety and difficult biodegradability, because as the energy demand is evolving, power transformers are being increasingly placed in cities, near the populations. Therefore, it was needed to find new alternative compounds, to better satisfy these requirements and protect both people and nature [2,22].

Therefore, the scientific community searched for safer and more ecological alternatives to mineral oil, and esters were one of the solutions found. They are biodegradable and non-toxic compounds, with a high flash and fire point, which answers the main problems imposed using mineral oil [21]. The esters can be either synthetic or natural.

Synthetic esters are the product of an esterification reaction that consists of a direct reaction between an alcohol molecule and a carboxylic acid molecule. The use of synthetic esters in the transformers industry is still somewhat limited, however, as the years have gone by, their use has increased, and today, transformers running on synthetic esters already reach rated voltages in the order of 400 kV [23]. Yet, synthetic esters are not fully biodegradable as they continue to present problems regarding environmental protection, so it is necessary to turn our attention to other substances, such as natural esters [24].

Natural esters began to be studied at the end of the 20th century. They are chemically composed of a main glycerol chain linked to three fatty acid groups that can differ from each other. The acid groups can be monounsaturated, polyunsaturated, or saturated. These differences define the properties of each ester. Esters are abundant all over the world, which ultimately makes it sustainable since it does not require the intensive exploitation of a particular region [24].

As esters arise as more eco-friendly alternatives to mineral oil, in the cooling and insulation of power transformers, studies have been made to understand and predict its thermal behavior and flow distribution [25]. Salama et al. [25] evaluated the transformer thermal performance while using 3 types of esters: 2 natural esters (Midel 1204 and Midel 1215) and 1 synthetic ester (Midel 7131), in comparison to mineral oil.

Four thermal-related properties of these esters were also evaluated: viscosity, thermal conductivity, specific heat capacity and density [25]. Figure 7 shows the top oil temperature and hot-spot winding temperature for the 3 esters and mineral oil, at a power transformer. It is shown that using the mineral oil, both temperatures are lower than using any of the esters. Among the esters, the Midel 7131 shows a better cooling performance.

The authors [25] also calculated the daily loss of life for each fluid, and by analyzing Figure 8, it is noted that mineral oil presents a high loss of life, while Midel 7131 guarantees a lower loss of life. Therefore, this study appears as a good example to observe that the use of esters as insulating fluid in power transformers, gives a performance similar to mineral oil, and is better for the power transformer in terms of its life.

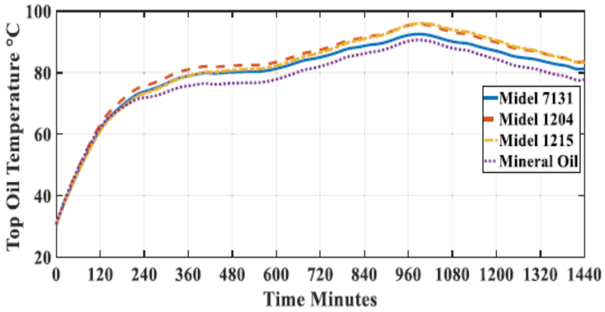

a)

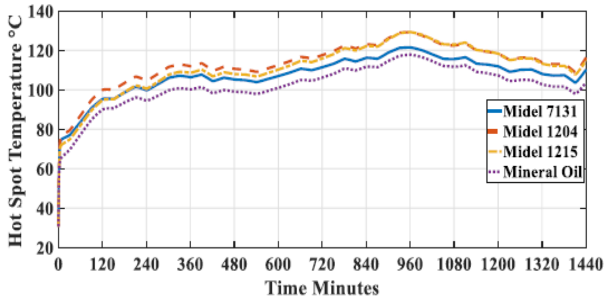

b)

Figure 7 - Evolution of temperature considering different fluids at a PT (mineral oil, Midel 7131, Midel 1204, and Midel 1215); a) Top oil temperature and b) Hot spot temperature [25]

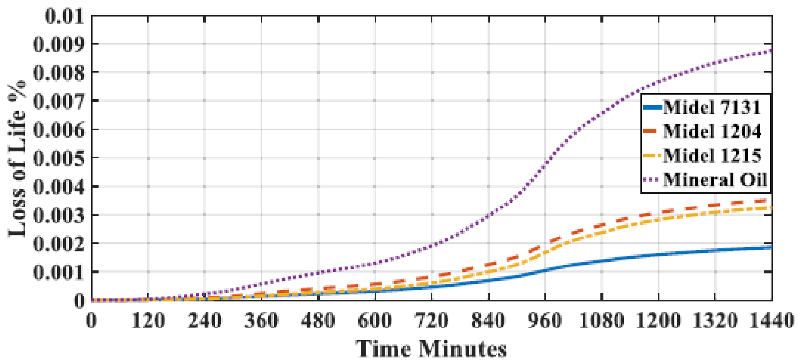

Figure 8 – Transformer daily loss of life when considering different cooling fluids: mineral oil, Midel 7131, Midel 1204, and Midel 1215 (at a Power transformer; [25]*)*

2.4 CFD modeling

In order to predict the fluid-flow and the thermal phenomena in a quantitative way, computational fluid dynamics (CFD) are often used [26]. The calculations depend on the properties of the fluid, the geometry of the flow, and the boundary conditions [26].

Over the past few years several numerical studies have been conducted to better understand both the fluid flow dynamics and the temperature distribution inside the windings, with special focus on identifying the hot-spot, since it is the hottest point within the transformer that dictates the ageing rate of the insulating material [17,18]. During experimental trials, a direct measurement of the temperature over the entire winding domain [17], is still complicated, and for that reason the CFD models are used to numerically simulate the thermal phenomena in the windings [27]. Jiahui Zhang and Xianguo Li [28], while studying the design parameters in oil cooling for disc-type transformer windings, concluded that the best cooling of the windings is achieved when the cooling flow distributions matches the heat generation distribution in the discs. They also made clear that it is necessary to perform a two-dimensional thermal analysis in winding discs, to find where is located the hot spot and what temperature it has [28].

Studies are performed concerning ON transformers (mineral [O]il with [N]atural convection) and OD transformers (mineral [O]il with [D]irected convection), where the main difference between them is that in ON the fluid flows due to buoyancy forces, while in OD its movement is forced by a pump. In a two part study [17,29], was made experimental and numerical investigations of the liquid flow and temperature distributions in a disc-type winding model of an ON and an OD transformer. It was concluded that for dimensional parameters, OD cooling presents a higher total liquid flow rate and higher dissipation of heat than ON cooling, and for dimensionless parameters, OD cooling have high Reynolds number (Re) and Richardson number (Ri) much smaller than 1, while ON cooling have lower Re and Ri typically larger than 1. It was also found that in OD cooling, the temperature and flow distributions are mainly controlled by Re, whereas in ON cooling, the temperature and flow are mainly controlled by Ri. Farinas *et al*. [30] studied the impact of the thermo-physical properties of oil on the cooling of transformers by natural convection, and they found that it is necessary, in order to properly replicate the cooling mechanism in CFD, to have temperature-dependent properties, namely density.

Leyla Raeisian et al. [31] developed a numerical scheme to optimize the distribution of power transformers' cooling system by examination of the transformers' design on their thermal management, and they concluded that the geometry also present a great influence on parameters such as the hot-spot temperature [31].

CFD is used in these simulations because it provides detailed and reliable results, even though the computational effort it requires is quite high.

2.5 Machine Learning

Machine learning was used in this work to build a tool that could predict the thermal behavior of a core-type power transformer, when defining its design parameters. This can be useful to study, more efficiently, the impact of the design and type of fluid in the windings' cooling.

Machine learning is a field of artificial intelligence that uses a set of algorithms to learn patterns in data, to predict outputs without being explicitly programmed on how to do so [32,33].

2.5.1 Machine learning approaches

There are 4 main approaches to machine learning: supervised learning, unsupervised learning, semi-supervised learning, and reinforcement learning.

- Supervised learning – Supervised learning uses labeled observation to train a model, that can map an input to an output (it predicts the output from a set of inputs). The input variables will influence the accuracy of predicted variables. Some examples of supervised learning methods are linear regressions, random forests, neural networks or support vector machines (SVM) [33–35];
- Unsupervised learning – This approach involves the training of unlabeled data, as the algorithm “looks” at the data and tries to find any relation/connection between it. It is, for instance, useful to reduce the number of features in a model (the dimensions reduction), when establishing relations between the data. Some of the most used methods in unsupervised learning are clustering algorithms [33,35];
- Semi-supervised learning – This approach is a middle term between the supervised and unsupervised approaches. The data scientists can “feed” the algorithm with labeled data to train (as in supervised learning), and then, the model explores the relations between it to find the best prediction method for that input data (as in unsupervised learning). It is helpful, for instance, when the training data is not enough to develop the algorithm [33,35];
- Reinforcement learning – Reinforcement learning is an approach similar to supervised learning, but this time it does not learn from static data, as the algorithm works on a trial-and-error basis, deciding its path from analyzing the results from tests that it performs until it reaches to the main objective [33,36].

The approach used in each situation will depend on the quantity and type of data available.

With the technological advances that are being witnessed in the world today, the field of Machine Learning has evolved, and it is becoming increasingly important and once the models can adapt to new data, it offers a wide range of application [32].

3 Materials and Methods

In this chapter the definition of the problem as well as the computational fluid dynamics approach used in this work are addressed. Then, a brief discussion on the machine learning approach used will be presented.

3.1 Problem definition

In the present work, it was intended to better understand how geometric features of the winding influences the thermal-hydraulic performance of an oil-filled or an ester-filled power transformer. It is expected that, once the thermal behaviors of the fluids in different geometric designs of the winding are compared, a conclusion can be reached on how to proceed in the application of natural ester, for the construction of more compact power transformers (MVA/ton) using the already widely implemented design rules related to mineral oil.

For that, the cooling phenomena inside a zig-zag core-type winding was simulated considering a geometry with 56 discs distributed by 7 passes (Figure 9, using mineral oil or natural ester as cooling fluid).

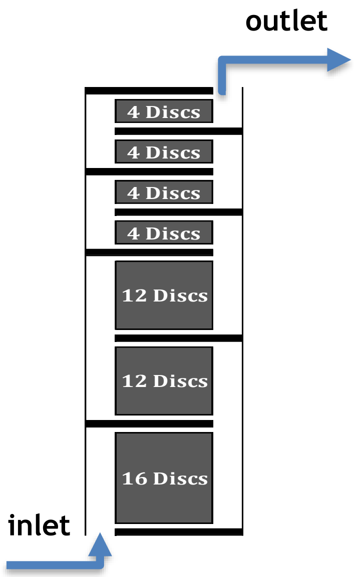

Figure 9 - Geometry of the studied core-type winding

The cold fluid enters the inlet (Figure 9) with a uniform velocity and temperature (bottom oil temperature) and flows through the winding removing the heat from the discs. The 7 passes of the winding are divided by pressboard washers that work as a thermal insulating and physical barrier to the fluid, directing its flow. After going through all the passes, the fluid exits by the outlet with a top oil temperature, that is the fluid's temperature at the top of the winding, following to external cooling circuit (not simulated). In this work the effectiveness and behavior of 2 different fluids (mineral oil Nynas Nytro TAURUS and natural ester Cargill

FR3) was evaluated in the internal cooling of a core-type power transformer, for different combinations of the axial and radial channels' dimension, and different entrance velocities. To confirm the validity of the numerical model to be implemented, a simple validation exercise was performed (Annex A).

3.2 Thermohydraulic simulations

3.2.1 Geometry design

A major part of the heat generated inside a power transformer is produced in the windings.

3D representation

The winding does not have a fully axi-symmetric geometry, but their tangentially repeated divisions (represented in Figure 10) define some symmetry plans, that enables the reduction of computational requirements without compromising the results, while studying the cooling of the winding.

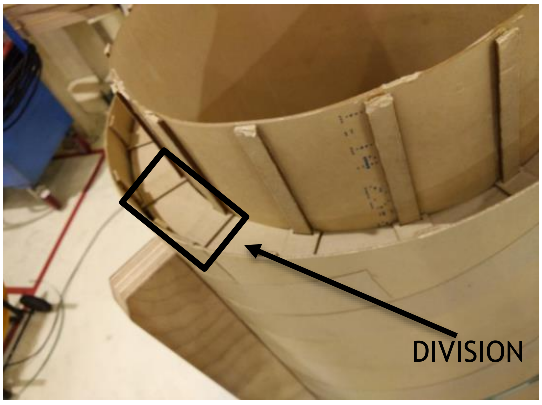

Figure 10 - Real winding showing tangentially repeated (16x) divisions

A 3D geometry of the winding, representing the repeated division, is represented in Figure 11.

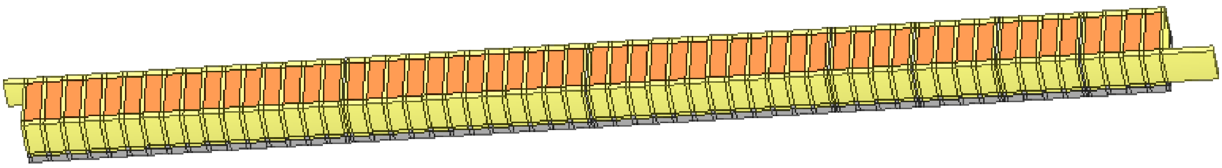

Figure 11 - 3D Geometry of one division of the winding

This geometry represents 1/16 of the total winding, and it allows to reduce the computing effort in the calculations. However, it stills requires heavy and high computational resources to obtain adequate and on-time results (regarding the available time to execute the work). To overcome this obstacle, the simplification of the 3D geometry into 2D was considered, assuming the fully axisymmetry.

2D axisymmetric representation

A 2D axisymmetric geometry was built, based on the 3D geometry shown in Figure 11. The geometry was built in Ansys SpaceClaim 2021 R2, considering the dimensions of a real winding according to Figure 12. It considers values of the size of the elements of a real winding from a core-type power transformer experimental setup owned by Efacec.

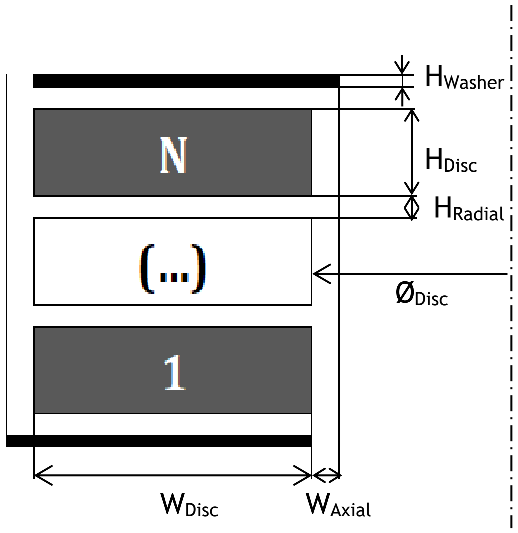

Dimension	Size / mm
H_{Disc}	15.60
W_{Disc}	43.85
H_{Washer}	2
W_{Axial}	6
$Ø_{Disc}$	462

Figure 12 - Schematic of the discs' dimensions inside a real winding

The size of the radial ducts is not constant, as it will vary depending on the arrangement of the winding as represented in Figure 13. Figure 13 shows the 2D geometry designed.

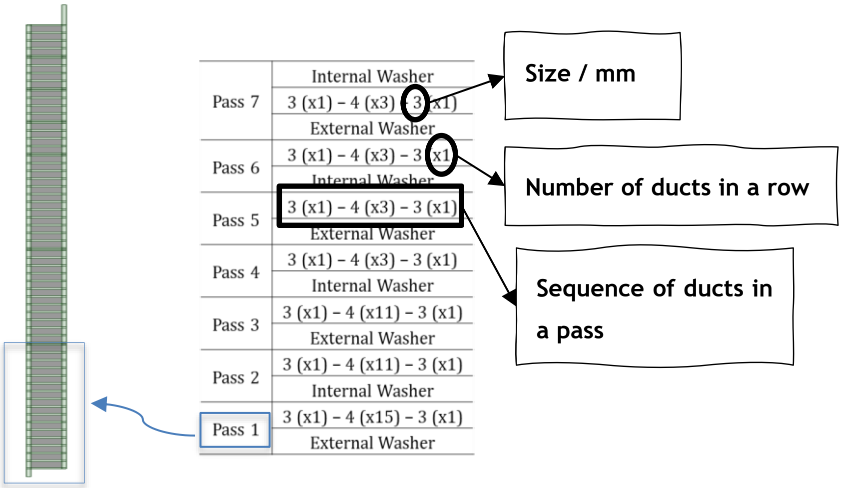

Figure 13 - 2D Geometry of the winding and radial duct sizes

3.2.2 Simulations configurations

The internal cooling of the winding was simulated in ANSYS Fluent 2021 R2 in steady state and laminar regime. A total of 108 simulations were performed, 54 of them concerning the fluid flow and other 54 concerning the thermohydraulic behavior, all in steady state. This division between hydraulic and thermohydraulic was made to study the influence of the heat exchange on the pressure drop of the fluid flow along the winding.

From the first set of 54 (hydraulic simulations), 27 concerned the mineral oil as cooling fluid (varying 3 radial channel sizes, 3 axial channel sizes, and 3 Reynolds numbers), and the other 27 simulations were replicated from the former but considering natural ester instead of mineral oil. Similar reasoning was followed for the second set of 54 simulations now considering the heat transfer phenomena.

Boundary conditions

The boundary conditions considered in the model are shown in Table 2.

Table 2 - Boundary conditions

Boundary Type	Momentum			Thermal	
	Boundary Condition	v_0 / m s^{-1}	P_0 / Pa	Boundary Condition	T_0 / °C
Inlet	Velocity	Input parameter	-	Temperature	43.35
Outlet	Pressure	-	0	-	Backflow: 26.85
Disc Wall	No Slip	-	-	Coupled	-
Winding wall	No Slip	-	-	Adiabatic	-

At the inlet, the fluid enters the winding with a uniform velocity (in all simulations) and uniform temperature (only in thermohydraulic simulations). At the outlet domain, the Gauge pressure was set to 0 Pa, for the momentum equation, and the backflow temperature was kept as default (26.85 ºC), for the energy equation.

As momentum boundary condition of the walls (of the discs and winding) a *No-Slip* condition was considered, specifying that the fluid in contact with the walls is immobile, i.e., it has null velocity (chapter 43.7.23 from [37]).

The thermal boundary condition of the disc wall was set as coupled (chapter 7.4.15.5.8. from [37]). The thermal boundary condition of the winding's wall was set as adiabatic because these walls have null heat flux.

The model assumptions and numerical procedures considered in the hydraulic and thermohydraulic simulations are described in the following subsection.

Hydraulic simulations – model assumptions and numerical procedures

The cases in which isothermal fluid flow was studied, were defined in ANSYS Fluent software and, were initialized by defining the state as stationary and considering gravity in the opposite direction to the flow at the winding entrance. The value set for gravitational acceleration was 9.81 m·s^{-2}.

The turbulence model was defined as laminar, energy was turned off, and the materials were created. The fluid domain is composed of mineral oil or natural ester. For the first 27 simulations Nynas Nytro TAURUS mineral oil was used and for the second group of 27 simulations it was used the natural ester Cargill FR3. Both fluids were defined with the characteristic properties at a reference temperature (i.e., 60 ºC , Table 3). Concerning the solid materials, copper and pressboard were created, bearing in mind that, for the isothermal fluid flow model, the properties of these materials are irrelevant, since they work only as a physical barrier.

Table 3 –Properties of mineral oil and natural ester at 60 ºC

Fluid	μ / kg m^{-1}s^{-1}	ρ / kg m^{-3}	*Cp* / J kg^{-1}K^{-1}	*k* / W m^{-1}K^{-1}
Mineral Oil	4.59×10^{-3}	846.40	2063	0.1298
Natural Ester	1.71×10^{-2}	893.68	2309	0.1527

For the methods, concerning the pressure-velocity coupling, the scheme used was the coupled algorithm, once it guarantees a more robust and efficient single-phase implementation for flows in steady-state, in comparison to segregated solution schemes, and once it is intended to study the pressure drop along the winding, this scheme is more appropriate [38]. The considered flux-type was the default method selected by ANSYS Fluent solver, *Rhie-Chow: distance-based*.

Concerning spatial discretization, the gradient method used was the *Least Squares Cell-Based*, also considered by ANSYS Fluent solver as the default method, and the selected pressure method was *PRESTO!*, since it is a method that works well with strong body forces, such as gravity and with it, the discretization gives more accurate results since interpolation errors and pressure gradient assumptions on boundaries are avoided [37,39]. The scheme selected to solve the momentum was the *Second Order Upwind* [39].

Concerning the solution controls, the flow Courant number was defined as 1. The flow Courant number relates the flow velocity v, a representative time step of the simulation Δt, and the characteristic size of the mesh cell Δh as shown in Equation 2 [40].

$$C = \frac{v\Delta t}{\Delta h} \tag{2}$$

The Courant number represents the amount of fluid that goes through a grid cell in a unit of time, and if that number is larger than one, it means that the fluid travels through more than one cell in a time step, making the solution less accurate, but reducing the computing time of the simulation [40]. The explicit relaxation factors and under-relaxation factors were maintained with the default values of 0.5 and 1, respectively.

In terms of residuals, for the Continuity, x-velocity, and y-velocity, these were defined as 10^{-6}.

Thermohydraulic simulations – model assumptions and numerical procedures

For the thermohydraulic simulations, the energy equation was activated, and the fluids were defined with the properties of real fluids described by their respective User Defined Functions (i.e., UDF's, Annex B). The thermal conductivity of the pressboard was set to 0.16 W m^{-1} K^{-1}, and for the discs it was set as orthotropic as shown in Figure 14. The rest of the properties were kept as default. Note that, the thermal conductivities of the discs are the effective thermal conductivities of a mixture of copper and insulating paper that compose the winding turns.

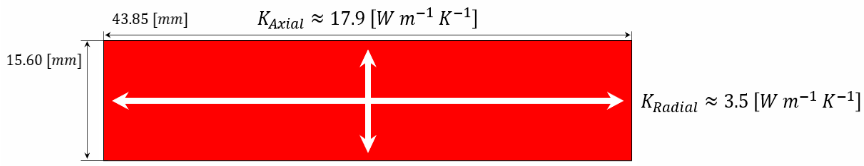

Figure 14 – Dimensions and orthotropic thermal conductivity of each disc

The fluid cell zones were defined by mineral oil or natural ester. The solid cell zones were defined by a copper - paper hybrid material in the disc zone. However, for the discs, a source term was added, following the distribution present in Annex C.

Besides all the definitions regarding the hydraulic simulations, in the thermohydraulic studies, additional definitions were necessary for the scheme to solve the energy. Again, the Second *Order Upwind* was set, because it offers a better accuracy in the calculation of the energy. The residuals of energy were set to 10^{-9}. The Courant number, explicit relaxation factors and under-relaxation factors were kept with the default values, except for the simulations with the lower Reynolds number for the mineral oil. The thermohydraulic simulations for mineral oil with the lowest velocity presented some difficulties to convergence, and to facilitate the convergence the following strategy was taken. First, the Courant number was heightened to 200, to promote the stability of the residuals. Then, once the residuals were stable, the Courant number was successively lowered every time the residuals stabilized until a Courant number of 0.01. Also, the explicit relaxation factor of momentum was successively lowered from 0.5 to 0.01 to help decrease the residuals until they converge.

3.2.3 Mesh independence tests

After the 2D geometry was built, the next step was to perform mesh independence tests to guarantee the reliability of the results. The mesh associated with the 3D geometry served as a starting point in the construction of the less refined mesh used in the independence tests.

The meshes built for the independence tests were based on changing the number of mesh divisions of 6 different surfaces of the geometry: disc width, disc height, axial channel width, radial channel height, inlet and outlet, and that variation followed the conditions in Table 4.

Table 4 – Meshes characteristics

Mesh	Disc width	Disc height	Axial channel width	Radial channel height	Inlet	Outlet	Number of elements
1	48	31	17	13	37	53	12928
2	75	50	45	30	45	75	45000
3	100	70	60	45	50	100	83800
4	120	90	80	60	50	100	138000
5	140	110	100	80	50	100	208800
6	160	130	120	100	50	100	294000

To simulate the problem with a refined mesh in all geometry requires a high computational performance and simulation time. During this work, both requirements were limited, and so, to perform the mesh independence tests, it was built a small geometry that encompassed the first 3 discs. For this geometry, the average and maximum temperatures in each disc, and the temperature profile along the top edge of the first disc was taken to compare results between design points. The mesh independence tests were performed considering the source terms of the first 3 discs described in Table 26 in Annex C, and the simulation configurations described in Annex D.

The results of the average and maximum temperature in each disc are shown in Table 5. The temperature profiles in the top edge of the first disc and the considered geometry (for the tests) are represented in Figure 15.

Table 5 - Average and maximum temperature of the discs obtained with different meshes

	Average temperature / °C			Maximum temperature / °C		
Mesh	Disc 1	Disc 2	Disc 3	Disc 1	Disc 2	Disc 3
1	53.27	52.59	52.6	55.37	54.47	54.26
2	53.40	52.85	52.68	55.50	54.75	54.36
3	53.51	52.97	52.69	55.62	54.87	54.37
4	53.59	53.03	52.69	55.69	54.91	54.37
5	53.66	53.06	52.68	55.76	54.95	54.36
6	53.71	53.07	52.68	55.81	54.96	54.36

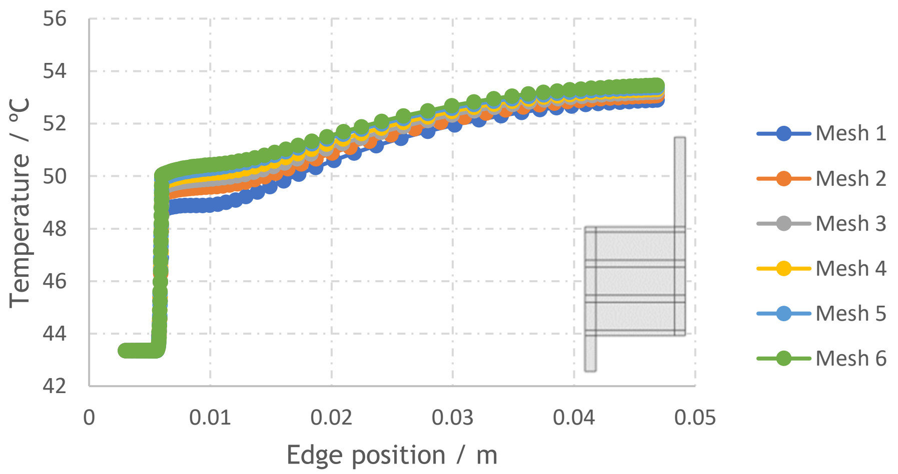

Figure 15 - Temperature profiles in the top edge of the first disc

As a selection criterion, the difference of one Celsius degree (i.e., the accuracy of an optical fiber probe [41]) in the average and maximum disc temperature was acceptable to validate the results between meshes. From Table 5, it is possible to conclude that between Mesh 1 and 6 a maximum deviation of 0.5 °C is observed in the maximum disc temperatures. Figure 15 shows that as the refinement of the mesh increases, the temperature profile variation decreases, as expected. So, a larger deviation is observed between the results of Mesh 1 and Mesh 2. As the second mesh already represents too high computation time, for a complete geometry of the winding, (about 14 hours) relatively to the time existent to execute the work, and because the maximum deviation of the disc temperature between the meshes, is lower than 1 ºC, it was chosen the first mesh to continue the work and proceed to the main simulations even knowing that it would not be the best to represent the intended phenomena. The selected mesh is represented in Figure 16.

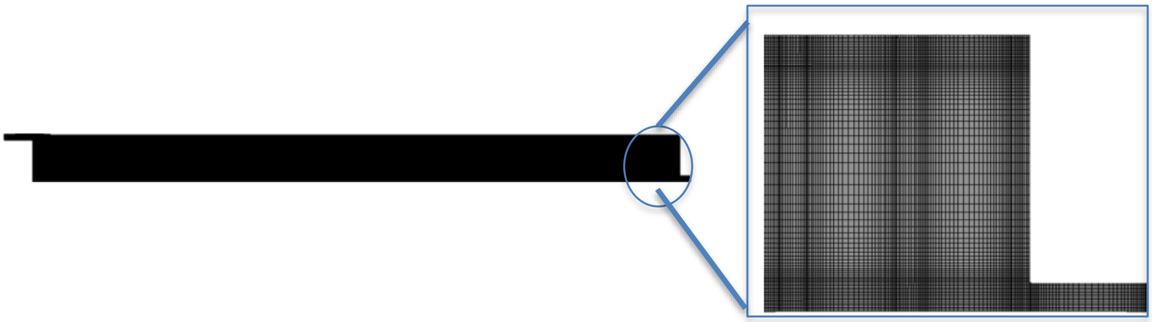

Figure 16 - Graphic Representation of the selected mesh

The numerical results obtained with the bi and tridimensional approaches were validated against experimental data, as described below.

3.2.4 2D and 3D Validation

To validate the assumption that an axi-symmetric 2D geometry would be representative of the winding, before proceeding with the main parametric simulations, a validation exercise was performed, where first, a simulation was made in axi-symmetric 2D and then in 3D, with the same conditions. Secondly, the numerical results were compared with experimental values previously obtained by Efacec, which consists of the average and maximum temperature rise registered by optical fibers located between discs (a total of 8 locations). For both axisymmetric 2D and 3D geometries, the source terms of each disc were defined according to Table 26 presented in Annex C. Additionally, in the tridimensional simulation case, a tangential conductivity of 367.35 W $m^{-1}K^{-1}$ was used (further calculations details in Annex E). The boundary conditions of the validation simulations are the same as in Table 2, with exception of the inlet velocity, which was defined as 0.19 m s^{-1} .

The temperature rise in the discs as given by Equation 3 and represents the difference between the measured (computed) temperature and the temperature of the environment, i.e., 25 ºC [6] .

$$Temperature\ rise = T_{measured} - T_{environment} \qquad (3)$$

Figure 17 shows the average, and the maximum temperature rises evaluated in each disc of both geometries and measured by the optical fibers in the experiment. By analyzing the figures, it is possible to conclude that there is an approximation between the results of both geometries and the experimental results. Concerning the average temperature rise, the maximum deviation between the results of axi-symmetric 2D and 3D geometries is 11% and the average deviation is 4%. In terms of the maximum temperature rise in the discs, the maximum deviation between both geometries results is 13% and the average deviation is 6%. These deviations are justified by the fact that the 2D geometry does not include some constructive elements of the windings, such as spacers that represent flow constraints. In fact, the inlet velocity was set in both models but, unlike the 2D geometry, the 3D geometry considers the spacers and consequently a lower entrance area. This means that the 2D geometry accounts for the same entrance velocity but higher fluid flowrate, which promotes lower temperatures in the 2D geometry.

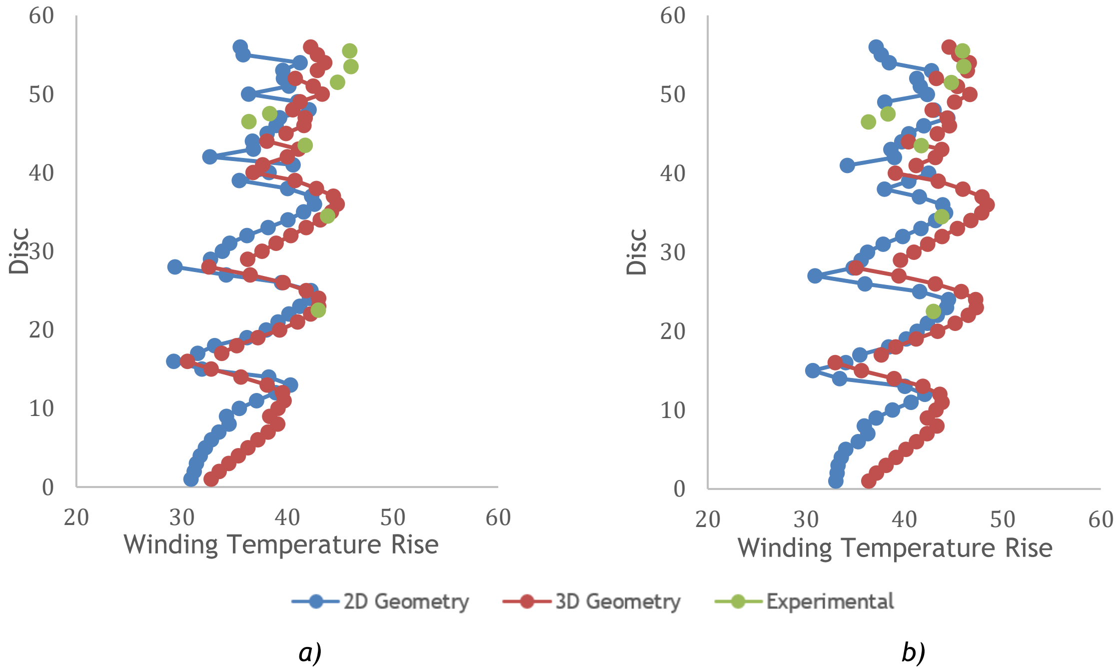

Figure 17 - a) Average temperature rise in the discs, b) Maximum temperature rise in the discs

Comparing the experimental and numerical results, it is noted that, for the maximum temperature rise in the discs, the maximum deviation happens in disc 56, relates the 2D geometry and corresponds to 22%. For the average temperature rise in the discs, the maximum deviation is 19%, also in disc 56 of the 2D geometry.

So, bearing in mind the difference in the results, in the inlet flowrate, and the high computing requirements and the time available, it was chosen the 2D geometry to perform these work simulations, as it provides a valid approximation and representation of the cooling phenomena happening in the winding, particularly in relative terms, as expected from the parametric variations.

3.2.5 Parameters' setting

In this work was intended to study a set of input parameters: axial channels' width, radial channels' height, and the Reynolds number at the inlet. To allow an automatic variation of these parameters, it was necessary to parametrize the geometry. For the axial channels, the tool “pull”, in ANSYS SpaceClaim 2021 R2, was used as a ruler dimension to specify the width of the channels as an input parameter. This tool allows to pull an edge in a direction, to increase or decrease its distance relative to a point. Figure 18 shows the definition of the right axial channel width as a parameter.

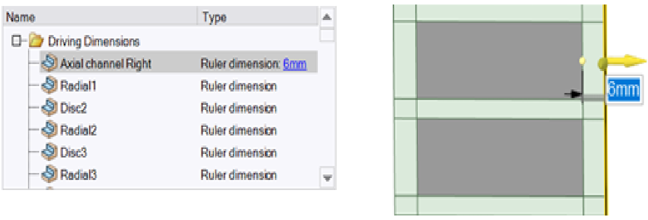

Figure 18 - Axial channel ruler dimension

For the radial channel it was used the tool “move” of ANSYS SpaceClaim 2021 R2. The “move” tool allows to move an edge in relation to another, increasing or decreasing the distance between them. This distance was also defined as a ruler dimension, to turn it into an input parameter (Figure 19).

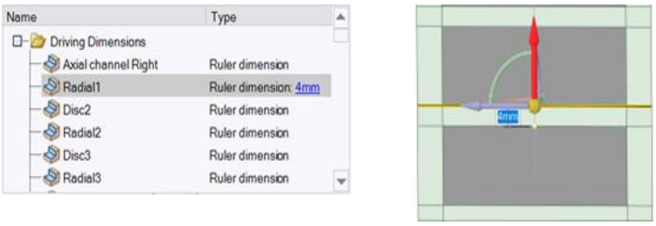

Figure 19 - Radial channel ruler dimension

The obstacle of this tool was when increasing the size of the radial channel, the disc size was decreased. To solve that problem, each disc height was also defined as a ruler dimension parameter, with the tool “move”, to avoid the deformation of the discs while changing the size of the channels.

Once the geometric input parameters were defined, it was necessary to define the edge sizing of each section, in Meshing, as input parameters too, so the mesh would automatically adapt to the new geometry, according to the distribution presented in Table 6.

Table 6 - Radial and axial channels' number of divisions

	Axial channel			Radial channel		
Size / mm	6	7	8	4	5	6
Number of divisions	17	19	21	13	15	17

The last parameter intended to change was the Reynolds number at the inlet, and for that, were selected 3 velocities, each from 3 different core-type power transformers, operating in forced convection, that were built and commercialized by Efacec. The selected velocities were 0.04, 0.11 and 0.29 m s^{-1} and they concern the mineral oil as fluid. So, for those velocities and an oil temperature of 60 ºC, the respective Reynolds numbers were calculated according to Equation 4 [42].

$$Re = \frac{\rho v D_h}{\mu} \tag{4}$$

considering ρ and μ the density and dynamic viscosity, respectively, at 60 ºC (Table 3), and the D_h the hydraulic diameter, which is two times the considered axial channel size (6 mm).

For the mineral oil, the calculated Re were 79, 247 and 643. The same values of Reynolds numbers were assumed in the studies with natural ester. The mineral oil and the natural ester have different properties, and for the same Reynolds number, the velocity will be different, so, the velocities obtained for natural ester, through Equation 4, were 0.13, 0.39 and 1.02 m/s.

With all the parameters already defined, a procedure was developed to automate the simulation of all the design points (described in Annex F).

3.3 Machine Learning

After performing the simulations, the results obtained were used to build a machine learning tool, that would automatically provide the expected thermal results after inserting the radial channel height, axial channel width, Reynolds number and the type of fluid. To enable the design of the machine learning tool, it was needed to follow a few steps, from data analysis to method selection and results prediction (see Figure 20)

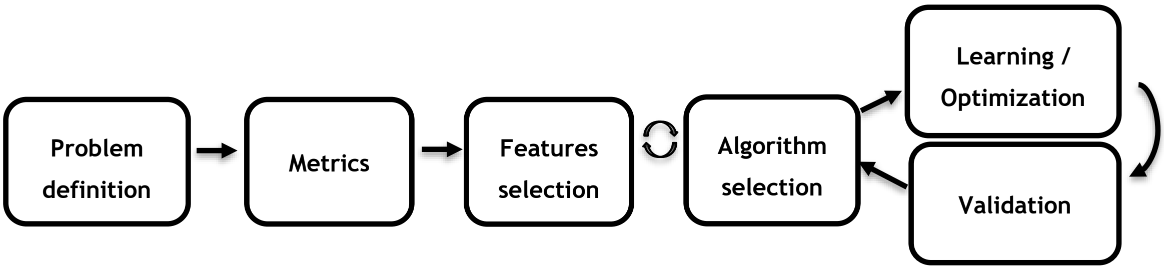

Figure 20 - Machine learning study framework

In the definition of the problem, it was necessary to understand what were the target variables (variables wanted to predict), what was going to be studied and what was the data structure. The objective was to compute the top-oil, average-winding, average-oil, and hot-spot temperatures, as well as the pressure drop, the hot-spot factor and the Nusselt number, for each set of inputs (radial channels' height and axial channels' width, Reynolds number and type of fluid), by clicking in a calculate button, like represented in Figure 21.

Concerning the metrics, it was necessary to define the best form to evaluate the existent data. In terms of the metrics used, the maximum error was chosen (considering the range of each result), since for these results, it was the metric that allowed a better understanding of the accuracy of the methods.

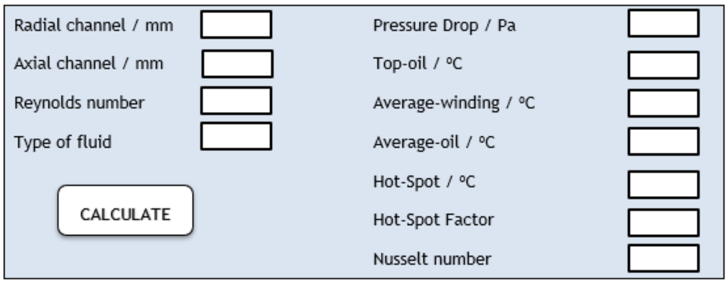

Figure 21 - Machine learning tool interface

The selection of the features and the algorithm selection are two steps that are strictly related to each other. Since the data set is quite small to train and test a 5-fold cross-validation resampling method was used. The cross-validation consists of randomly splitting the data into clusters of 70% to train and 30% to test on different iterations. The algorithm selection is an iterative process, where different algorithms are explored, as well as different parameters, using a technique called Grid Search, and their results are evaluated. The Grid Search consists of an exhaustive search on specified parameters for an estimator. The goal is to always improve and optimize every method and after validating it, see if there is any better algorithm/parameters set that can be used.

Since the objective is to predict labeled outputs from labeled inputs, the approach used is supervised learning. This learning approach is divided into two main categories of algorithms: classification and regression. The classification algorithms are used when the output variables are categories, such as “Red or Blue”, “True or false” or “Yes or No”. The regression algorithms are used when the output variables are continuous like “Temperature” or “Price” [35,36].

It was necessary to define the algorithm to use, by analyzing the scores of the defined metric (maximum error). It was tested linear regression, random forests, and support vector machine, and the respective errors were analyzed, and it was concluded that the algorithm that better-predicted results, was random forest. The random forest regressor consists of the creation of a group of trees (forest), and each one uses a random sample of the existent data to predict. With all the predictions of all trees performed, an average of them is made, thus giving rise to the random forest regressor [43]. This scheme is represented in Figure 22.

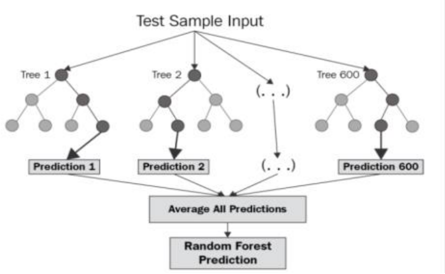

Figure 22 - Random Forest example (adapted from [44])

Finally, to build the interface, the Python library “tkinter” was used.

4 Results and discussion

The results in this chapter (in tables) are a selection used to demonstrate tendences of the thermal performance in the winding. All the results are shown in Annex G.

4.1 Hydraulic simulations

These simulations intended to determine the pressure drop of the fluid flow along all the winding for both mineral oil and natural ester.

Figure 23 shows the contours of the velocity magnitude inside the winding with 6 mm of radial and axial channels' height and width, respectively, and a Reynolds number of 79, for the mineral oil.

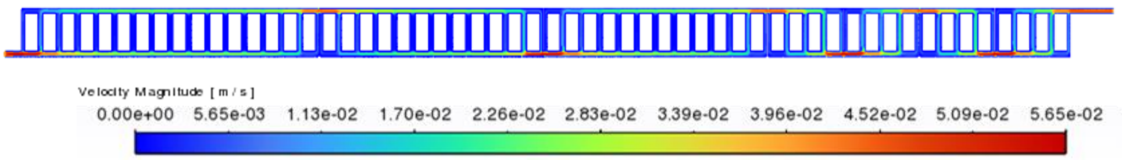

Figure 23 – Contours of velocity magnitude inside the winding (axial channel width: 6 mm, radial channel height: 6 mm, Re = 79, fluid: mineral oil)

The velocity distribution inside the winding is dependent of the inlet velocity, and the geometric features of the channels. Figure 24, Figure 25, and Figure 26 show the contours of velocity magnitude, obtained for different geometric and inlet velocity combinations. To facilitate the comparison of these changes, one specific zone of the winding was selected, that properly shows the influence of the parameters in the fluid flow. This zone comprises the last 4 passes with 4 discs each (Figure 9).

In Figure 24 is shown that the evaluated variation of the radial channels' height has a slight effect on the fluid velocity (average velocity for a radial channel height of 4 mm is 15 % higher) but not in the fluid flow behavior. In Figure 25 it is possible to see that the increase of the axial channels' width will provoke an increase, in 13%, of the average-velocity in the winding (is possible to see differences of the velocity in the zones marked with a black circle), and also increase the velocity of the fluid in some regions, namely in the radial channels (red circles). Nevertheless, the bigger difference, as expected, is noted when the Reynolds number is increased, as it is possible to see in Figure 26. With the increase of the inlet velocity, the fluid flow has more preferential paths, and so being less distributed along the ducts. The flow's behavior in hydraulic simulations can be better understood looking for the values of the pressure drop along the winding for a set of design points (Table 7, Table 8 and Table 9).

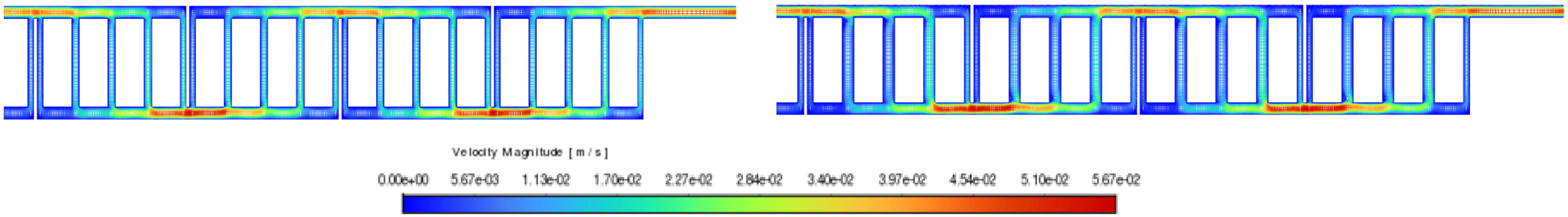

a) b)

Figure 24 - Contours of velocity magnitude inside the last four passes of two transformers with different radial channel height: a) 4 mm; and b) 6 mm (axial channel width: 6 mm; Re = 79, fluid: mineral oil)

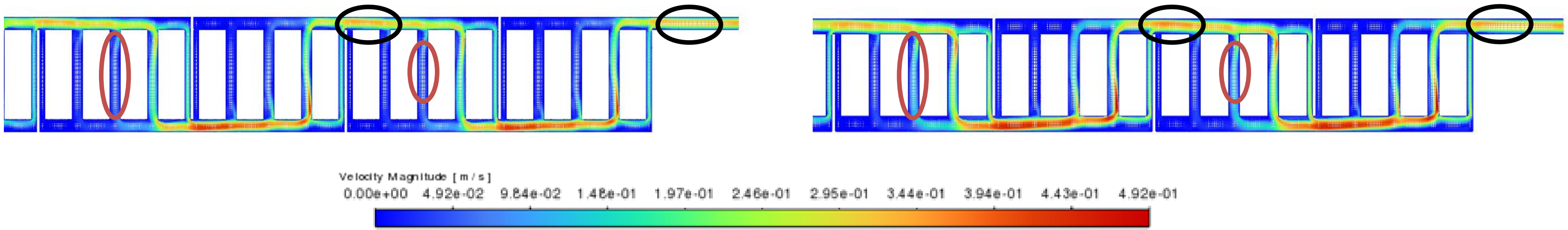

a) b)

Figure 25 - Contours of velocity magnitude inside the last four passes of two transformers with different axial channel width: a) 6 mm; and b) 8 mm (radial channel height: 6 mm; Re = 643, fluid: mineral oil)

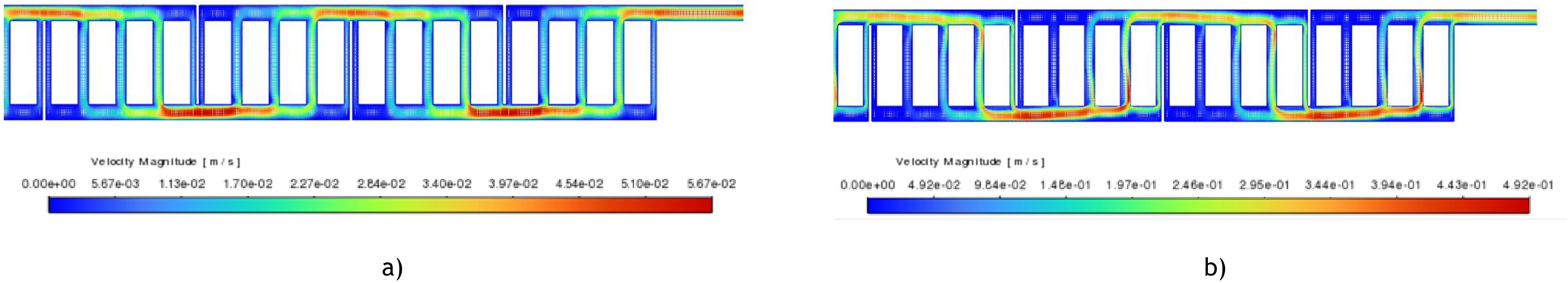

Figure 26 - Contours of velocity magnitude inside the last four passes of two transformers with different Reynolds numbers: a) 79; and b) 643 (radial channel height: 6 mm; axial channel width: 8 mm, fluid: mineral oil)

Table 7 - Variation of pressure drop with the increase of the radial channels' height (fluid: mineral oil)

Radial Channel / mm	Axial Channel / mm	Reynolds number	∆P / Pa
4	6	247	166.7
5	6	247	160.5
6	6	247	158.4

Table 8 - Variation of pressure drop with the increase of the axial channels' width (fluid: mineral oil)

Radial Channel / mm	Axial Channel / mm	Reynolds number	∆P / Pa
5	6	79	50.6
5	7	79	41.4
5	8	79	35.6

Table 9 - Variation of pressure drop with the increase of the Reynolds in the inlet (fluid: mineral oil)

Radial Channel / mm	Axial Channel / mm	Reynolds number	∆P / Pa
5	7	79	41.4
5	7	247	136.2
5	7	643	579.6

Analyzing Table 7, for the same Reynolds number and axial channels' width, it is possible to conclude that increasing the radial channels' height the pressure drop decreases (a maximum difference of ~10 % for both fluids). The same tendency happens when increasing only the axial channels' width, as seen in Table 8 (maximum difference of ~ 25 % for both fluids). Table 9 shows that, for a fixed radial channel's height and axial channels' width, as expected, the pressure drop will increase with Reynolds number increase. In average it increases 3.7 times for oil and 3.9 times for ester. The results obtained in all the simulations are shown in Annex G.

For the natural ester, the same tendencies were observed, but this time, as the properties of the ester are different from the mineral oil, at the same temperature, the values of the pressure drop were considerably different. In the hydraulic simulations, the properties of the materials were considered at a constant temperature of 60 ºC (Table 3).

As both dynamic viscosity and density of the natural ester are greater than the ones for mineral oil, it was expectable that the ester would promote more resistance to the flow, than the oil, and therefore, the pressure drop would be higher. This presumption was verified as it is shown in Table 10, Table 11 and Table 12. The pressure drop was in some cases, 13 times higher for the ester than for the oil, for the same design points.

Table 10 - Variation of pressure drop with the increase of the radial channels' height (fluid: natural ester)

Radial Channel / mm	Axial Channel / mm	Reynolds	DP / Pa
4	6	247	2203.9
5	6	247	2122.7
6	6	247	2095.2

Table 11 - Variation of pressure drop with the increase of the axial channels' width (fluid: natural ester)

Radial Channel / mm	Axial Channel / mm	Reynolds	DP / Pa
5	6	79	608.8
5	7	79	497.7
5	8	79	427.4

Table 12 - Variation of pressure drop with the increase of the Reynolds in the inlet (fluid: natural ester)

Radial Channel / mm	Axial Channel / mm	Reynolds	DP / Pa
5	7	79	497.7
5	7	247	1801.7
5	7	643	7576.1

In terms of the fluid flow patterns, the natural ester behaves like the mineral oil, only varying the velocity (explained in 3.2.5) as it is shown in the Figure 27, with the contours of velocity magnitude obtained in a winding with 6 mm of axial and radial ducts' size and a Reynolds number of 643.

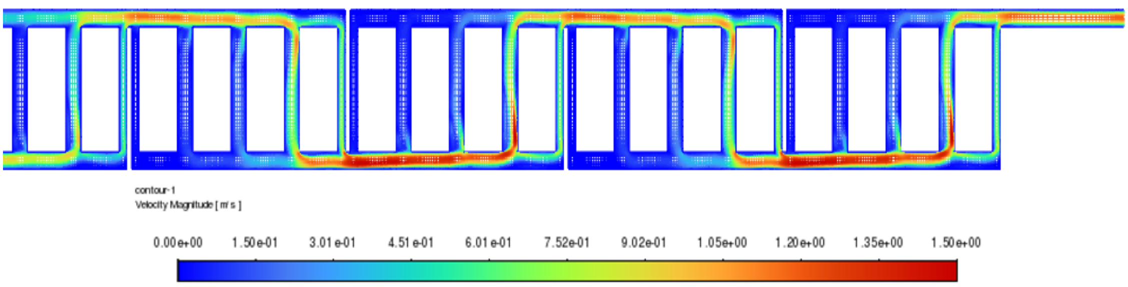

Figure 27 - Contours of velocity magnitude distribution inside the last 4 passes of a 6 mm axial and 6 mm radial channel transformer with Re = 643, using natural ester

4.2 Thermohydraulic simulations

When analyzing the results of the simulations concerning the thermohydraulic behavior, it is possible to discuss different aspects of the geometry features and the fluid effect on the cooling process of the winding.

Figure 28 shows an example of the pressure drop vs Reynolds number, for mineral oil and natural ester, considering different axial channels' width (fixed radial height). Further results obtained for different geometrical features are presented in Annex G, however, the tendencies are very similar to that observed in Figure 28. First, looking to the behavior of the pressure drop in thermohydraulic simulations, it is almost the same as for hydraulic only. The differences are on the values magnitude, once the simulation concerning hydraulics considered the properties of both the fluids at 60 °C, and for thermohydraulic their properties vary with temperature according to the respective UDF´s (Annex B). The average viscosity and density of each fluid are higher along the winding, and for that reason the pressure drop is also higher.

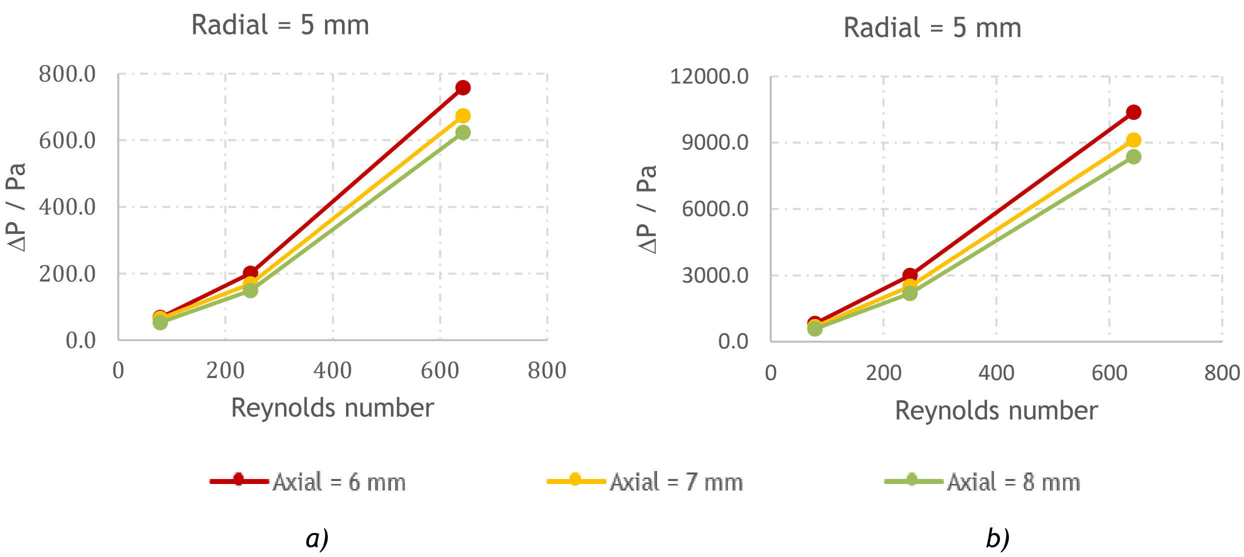

Figure 28 - Pressure drop as a function of the Reynolds number in the windings with different axial channels' width (radial channel height=5 mm), using: a) mineral oil and b) natural ester

Considering the thermohydraulic simulations, the output parameters to be analyzed were the top-oil, average-fluid, average-winding, and hot-spot temperatures, as well as the hot-spot factor and the Nusselt number.

Observing the contours of temperature inside the windings with the same geometric features, it is possible to analyze the effect of fluid type on the winding's cooling performance (Figure 29, Figure 30 and Figure 31).

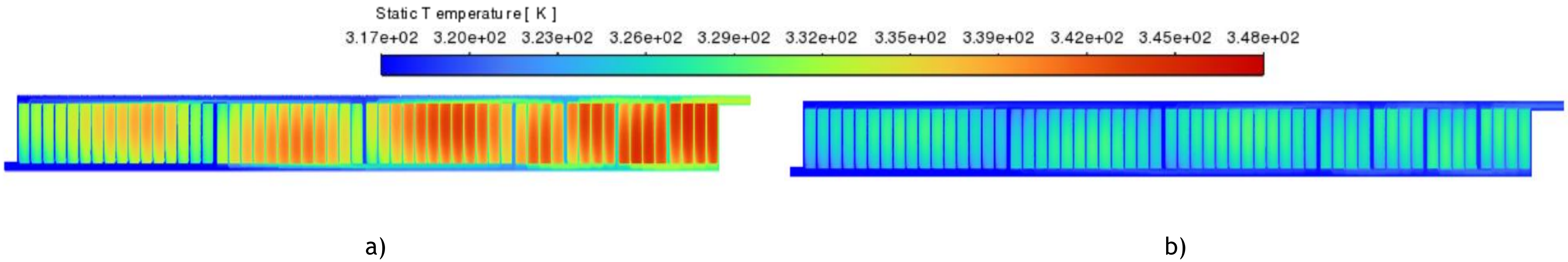

Figure 29 – Contours of temperature inside the winding for radial channels' height=4 mm, axial channels' width=6 mm, Re=247, using a) mineral oil; b) natural ester

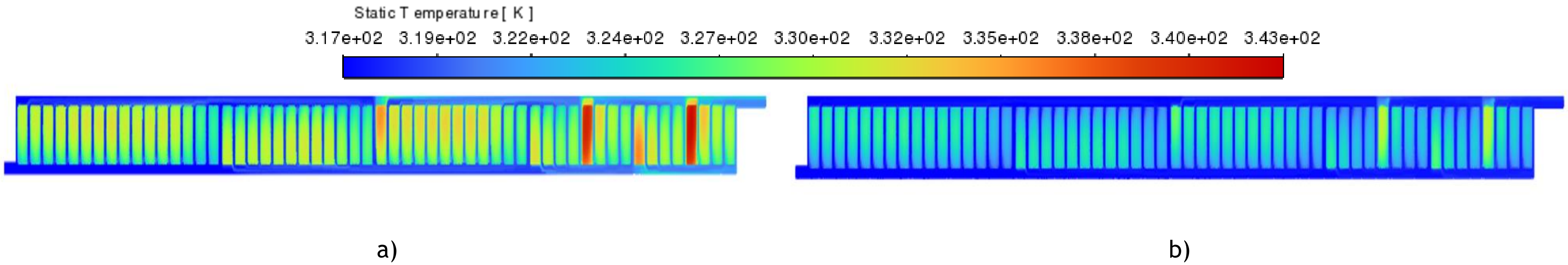

Figure 30 - Contours of temperature inside the winding for radial channels' height=6 mm, axial channels' width=8 mm, Re=643, using a) mineral oil; b) natural ester

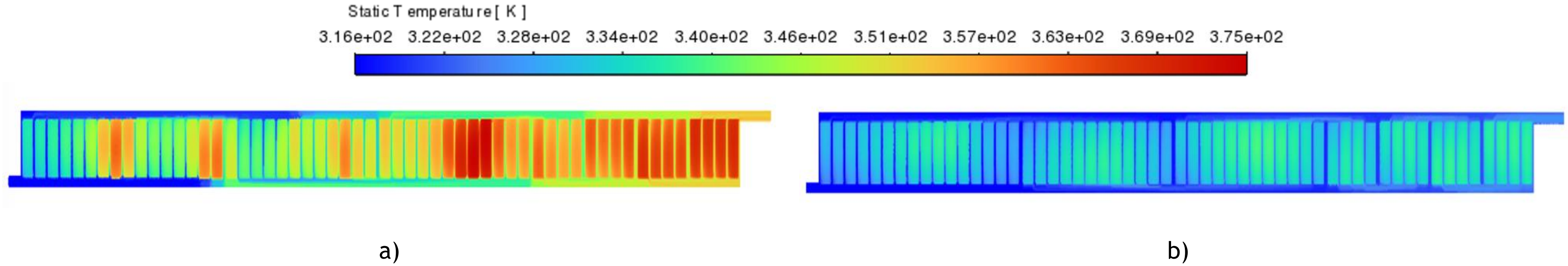

Figure 31 - Contours of temperature inside the winding for radial channels' height=5 mm, axial channels' width=7 mm, Re=79, using a) mineral oil; b) natural ester

Observing all the situations reported in the contours of temperature inside the winding for the two fluids, is possible to conclude that, for the same design points (including the same Re), natural ester presents a better cooling performance than the mineral oil, once the temperatures of the conductor are lower in all cases presented. Comparing the different contours, for lower velocities, the temperatures inside the winding will be higher, as expected. To further analyze the cooling phenomena inside the winding, results regarding each output parameter are analyzed in the following Table 13, Table 14 and Table 15.

Table 13 – Thermal results for different radial channels' height

Radial Channel mm	Axial Channel mm	Reynolds	Top-oil °C		Average-oil °C		Av.winding °C		Hot-spot °C		HSF		Nusselt number	
			oil	ester	oil	ester	oil	ester	oil	ester	oil	ester	oil	ester
4	**6**	**247**	59.5	47.1	52.2	45.6	64.1	53.1	72.2	56.4	1.01	1.18	5.83	6.28
5	**6**	**247**	59.5	47.1	52.6	45.8	65.1	53.6	72.8	58.0	0.98	1.29	5.64	5.81
6	**6**	**247**	59.5	47.1	54.8	46.3	66.4	54.2	78.8	60.1	1.29	1.45	4.93	5.34

Table 14 - Thermal results for different axial channels' width

Radial Channel mm	Axial Channel mm	Reynolds	Top-oil °C		Average-oil °C		Av.winding °C		Hot-spot °C		HSF		Nusselt number	
			oil	ester	oil	ester	oil	ester	oil	ester	oil	ester	oil	ester
5	**6**	**247**	59.5	47.1	52.6	45.8	65.1	53.6	72.8	58.0	0.98	1.29	5.6	5.8
5	**7**	**247**	57.2	46.6	51.1	45.4	63.3	53.1	70.5	56.3	1.02	1.20	5.2	5.5
5	**8**	**247**	55.5	46.2	50.1	45.1	62.1	52.7	68.8	55.8	1.05	1.20	4.9	5.2

Table 15 - Thermal results for different Reynolds number

Radial Channel mm	Axial Channel mm	Reynolds	Top-oil °C		Average-Oil °C		Av.winding °C		Hot-spot °C		HSF		Nusselt number	
			oil	ester	oil	ester	oil	ester	oil	ester	oil	ester	Oil	Ester
5	**7**	**79**	79.9	53.0	63.7	49.1	79.6	59.9	97.3	65.7	0.97	1.09	3.9	4.7
5	**7**	**247**	57.2	46.6	51.1	45.4	63.3	53.1	70.5	56.3	1.02	1.20	5.2	5.5
5	**7**	**643**	48.7	44.6	46.9	44.2	56.1	50.2	68.4	55.2	1.96	1.69	6.1	5.9

In the discussion of the results, the tendences of the values were calculated as relative errors, based on the results obtained for the consecutive variation of the inputs (Table 29 and Table 30). Looking to the top-oil temperature, as expected, it tends to decrease in average 28.8% for oil and 9.3% for ester, when maintaining the geometric parameters and the inlet temperature, but increasing the inlet velocity. Maintaining the Reynolds number, the only geometric property that influences the top-oil temperature is the width of the axial channels (increasing its size, the top-oil temperature decreases in average 3.7% for oil and 1.3% for ester), because in this case the flowrate is changed to maintain the Re (explained from Equation 5). By observing the energy balance to the fluid in the winding (Equation 6), only the axial channels influences it , as their width is represented by the A_{inlet} in the calculation of the mass flow-rate (Equation 5).

$$\dot{m} = \rho\, v\, A_{inlet} \cdot 3600 \qquad (5)$$

$$Q = \dot{m}\, C_p \left(T_{top-oil} - T_{bottom-oil}\right) \qquad (6)$$

Concerning the average fluid temperature, it is possible to conclude that it increases in average 2.3% for oil and 0.9% for ester with the increase of radial channels' height and decreases in average 2.6% for oil and 1% for ester, with the increase of the axial channels' width (as expected because the top-oil also decreases). It also decreases with the increase of the Reynolds number at the inlet (in average of 18.3% for ester and 5.8% for ester). For the first situation, the increase in the height of the radial channels, which are located between discs, leads to a greater amount of fluid receiving heat, while the fluid is more evenly distributed among the radial channels (Figure 24). Regarding the axial channels, as their width is increased, more flowrate is admitted to the winding (to maintain the same Re), resulting in lower top-oil and consequently lower average-oil (Equation 6).

Comparing the top-oil temperature and the average-oil temperature between the mineral oil and the natural ester, the ester has lower temperatures than the oil, in all the cases. In terms of the average-oil temperature, considering an inlet temperature of 43 ºC, the oil heats 3.82 times more than the ester. For the top-oil temperature, the oil heats 3.8 times more than the ester. Once the temperature of the fluid varies with the heat received from the discs, this difference is observed due to the different heat capacity of each fluid. As seen in Table 3, for the same temperature, the heat capacity of the natural ester is higher than the one of the mineral oil, so it is necessary more energy to increase the temperature of the natural ester in 1 ºC than for the mineral oil.

Regarding the discs, there are two thermal properties to analyze: the average-winding temperature and the hot-spot temperature. The first represents the average temperature of the discs throughout the winding, and the second is the highest temperature within the winding, which always occurs at the discs.

Looking first to the results of the average-winding temperature in Table 13, it is observed that as the height of the radial channels increases, the temperature of the discs also increases (1.15% for oil and 1.21% for ester). As the width of the axial channels increases, the average winding temperature decreases 2.1% for oil and 1.1% for ester. As expected, as the inlet velocity increases, more heat is removed from the discs to the fluid and consequently, the temperature of the discs decreases (in average 19.8% for oil and 9.5% for ester).

For the hot-spot temperature, as general rule and as expected, there is the same trend as for the average-winding temperature. The higher the average temperature of the discs, the higher will be their expected maximum temperature. However, the hot-spot temperature is a difficult property to predict, since its value will vary with some factors, such as the existence of recirculation zones, or certain geometric designs that provokes specific behaviors of the fluid flow. For this reason, there were situations, in the simulations made, where the hot-spot temperature results did not match to what was expected. These occasional situations were analyzed (e.g., Figure 32), where is shown the contours of the temperature within the last pass of the winding (Figure 32a), as well as the velocity magnitude contours (Figure 32b), in the same region, for ester, considering a Reynolds of 643, an axial channels' width and a radial channel's height of 6 mm.

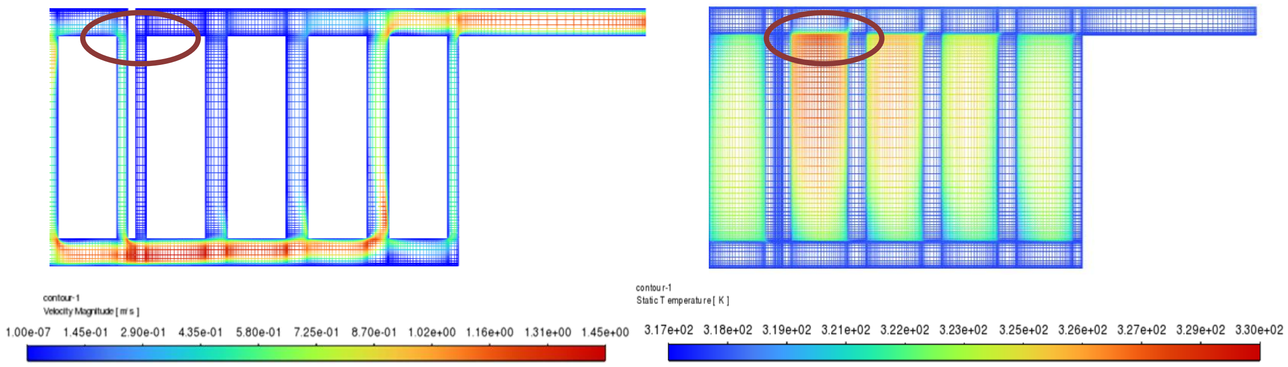

a) b)

Figure 32 – Contours of a) velocity magnitude distribution; b) temperature using natural ester as cooling fluid

The simulations for the higher Reynolds number and the same radial channels' height, showed an unexpected trend in the values of the hot-spot temperature, while increasing the axial channels' width. It was expected to follow the trend of the average winding temperature, but it was completely the opposite as possible to see in Table 16.

Table 16 – Variation of the hot spot temperature with the increase of axial channels' size

Radial channel mm	Axial channel mm	Reynolds number	Average winding °C	Hot-spot °C
6	6	643	50.64	54.75
6	7	643	50.56	56.42
6	8	643	50.56	57.95

Observing Figure 32 and comparing it to the values showed in Table 16, is possible to conclude that there is very little fluid flowing near the zone indicated by the red circle (hot-spot). If there is little fluid, there is almost no cooling, so the hot-spot temperatures will be even higher in these cases. This only happens for the higher velocities' situations, as the distribution of the fluid is not so uniform on the radial channels and the fluid concentrates more near the last discs of each pass, leaving the first discs less cooled (as possible to see in Figure 32 and Figure 26).

When comparing the average-winding temperature for the two fluids, it can be observed that when ester is used, the temperatures are in average 21.5% lower than when oil is used.

This can be explained looking to the Nusselt number. The Nusselt number is the ratio between the convective heat transfer and the conductive heat transfer (Equation 7, [42]) and the higher the Nusselt number, the more heat is dissipated by the discs by convection.

$$Nu = \frac{h\,L_C}{k} \tag{7}$$

The remaining parameter to analyze is the hot-spot factor (HSF; described by Equation 1; [16]). In the hot-spot factor equation, the average temperature of the fluid is calculated using the top-oil and bottom-oil temperatures, because experimentally is not possible to obtain the average-oil temperature like in the numerical simulations. In Table 29 and Table 30, the HSF assumes, in the majority of times, values between 1 and 2. Values below 1 means that the maximum gradient is lower than the average winding-to-oil gradient (Figure 5). On the other hand, an HSF value above 2 implies that the hot spot starts to become too high relative to the top-oil, and since transformers are dimensioned taking into account the hot-spot temperature, a very high HSF value implies a considerable concern in dimensioning the respective transformer to reduce the impact of the hot-spot.

4.3 Machine learning

4.3.1 Tool performance

The results were obtained by CFD numerical simulations, and from there it was off to the creation of the machine learning tool. As the variables to analyze are continuous, regression algorithms were used, more specifically the random forest regressor. Since the data in this work is not plentiful enough to allow a more accurate prediction, this came up as a preliminary analysis on how this type of methods can predict the thermal performance of a core-type PT. To enable the most accurate prediction possible, the acceptable maximum error for each predicted parameter was set at 20%. The maximum error obtained for each output parameter using the random forest regressor (with 100 estimators) is described in Table 17.

Table 17 - Maximum error for the predicted parameters using Random Forest

Predicted parameter	Maximum error / %
Pressure Drop	9
Top-Oil Temperature	10
Average-winding	21
Average-oil	10
Hot-spot temperature	14
Hot-spot factor	70
Nusselt number	16

Observing Table 17, it is possible to conclude that only the average-winding and the hot-spot factor present a maximum error percentage above 20%. For the hot-spot factor, the error was too high, so it was needed to find a different strategy to predict it. Ultimately the random forest with 800 estimators (trees) was chosen as the method that provided the best prediction of the output, as the error was reduced to nearly 61%. This maximum error is high, presumably, because the hot-spot factor considers other variables with an already associated error. It is expected that with more data, the machine learning tool response improves, and the error considerably decreases.

The results obtained from the numerical study were fed to the machine learning algorithm, to build a tool capable of predicting the results, when giving the inputs on the axial channels' width, radial channels' height, Reynolds number at the inlet, and type of fluid. The code used to execute the machine learning tool is present in Annex H. Figure 33 shows the usage of the machine learning tool.

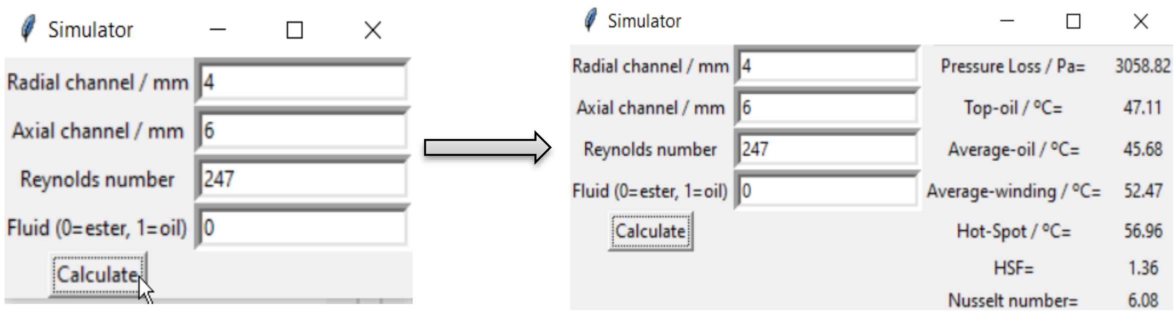

Figure 33 - Example of the tool usage

Table 18 compares the values obtained by the machine learning tool, to the ones obtained in the thermohydraulic simulations, in CFD, for the same set of inputs (the same as in Figure 33).

Table 18 – Comparison between the results obtained using machine learning and CFD

	Pressure Drop / Pa	Top-oil / ºC	Average Fluid / ºC	Average winding / ºC	Hot-spot / ºC	HSF	Nusselt number
Machine Learning	3058.82	47.11	45.68	52.47	56.96	1.36	6.08
CFD	3125.86	47.13	45.61	53.1	56.4	1.18	6.28
Deviation	2.14 %	0.04 %	0.15%	1.19 %	0.99%	15%	3.18 %

In Table 18, it is possible to see that the machine learning tool predicts, with considerable accuracy, the values obtained through CFD, with exception of the HSF, whose error is high as expected from the maximum error computed previously.

This tool should only be used on the range of values that were used for training, since it is not prepared to give an adequate response for Reynolds numbers, or channels' sizes outside this data range. Once again, it is necessary to give more data to the algorithm to assure this tool is capable to give a wider response.

4.3.2 Practical usage

In order to demonstrate a direct application of the machine learning tool, a transformer retrofilling exercise was performed. The goal was, just by using the machine learning tool, obtain the pressure drop vs. flowrate curves for the two fluids (mineral oil and natural ester), using the 3 Reynolds values trained by the tool, an axial channels' width of 7 mm and radial channels' height of 5 mm. By adding the values obtained to others from pressure drop vs. flowrate curves provided by Efacec, referring to the pressure drop of the external system of an experimental installation, the system curves for the fluids were generated (to obtain the system's pressure drop for this example, was needed to use a tool that allowed to know what was the pressure drop of all the cooling circuit). With the system curves acquired, the curves of a specific pump, for ester and oil, were used with the system curves to get the respective operating points. The purpose of the exercise would be to compare the thermohydraulic behavior of a transformer for the operating points of each fluid using the same pump. For the exact same transformer (and inherent pump), it was possible to accurately and rapidly find the operating points (fluid flowrate and pressure drop) of the transformer when using from mineral oil and natural ester. Figure 34 shows the operating points obtained for each fluid.

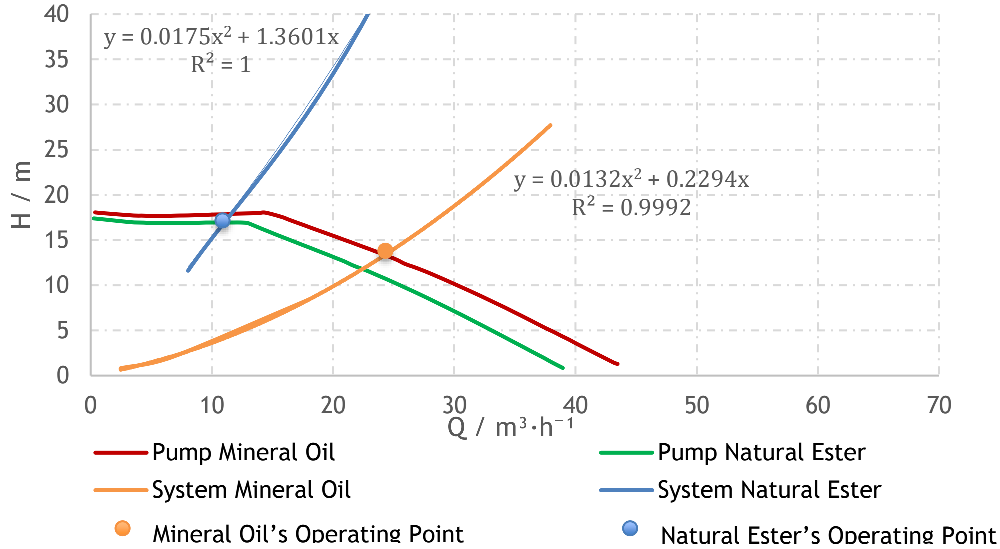

Figure 34 - Mineral oil and natural ester operating points

Although the operating flowrate and corresponding Re could be found, it was not possible to finish the exercise. The machine learning tool is not yet suitable for predicting (with enough accuracy) the values of the thermohydraulic results (top-oil, average-oil, average-winding and hot-spot temperatures) for the flowrates/Reynolds of the fluids' operating points. This tool only provides good approximations and valid results for the trained flowrate/Reynolds values and needs further calibration. Yet, the developed simulator is a very promising tool to use, for instance, in this type of analysis, provided that the tool is enriched with more necessary design point to ensure its robustness.

5 Conclusion

In this work, the influence of windings design in the internal cooling of a core-type power transformer was studied considering mineral oil and natural ester as cooling fluid. For that, a bidimensional CFD approach was used to obtain the values of pressure drop in the winding, the Nusselt number, hot-spot factor and the temperatures of the top-oil , average-oil, average-winding, and the hot-spot. The simulations were performed for combinations of radial channels' height (4, 5 and 6 mm), axial channels' width (6, 7 and 8 mm), Reynolds numbers (of 79, 247, and 643), and for different fluids (mineral oil and natural ester). A bi- and tridimensional approaches were implemented and validated with experimental results. Furthermore, the numerical results were fed to a machine learning algorithm to obtain a predictive model of 7 parameters representative of winding cooling performance.

First the simulations were performed, initially without the existence of heat transfer and later with heat transfer. It was observed that the existence of heat transfer does not affect the fluid flow patterns along the winding, affecting only the values magnitude (~30% higher considering heat transfer for both oil and ester; related with the fluid properties variation with temperature). Comparing the pressure drop values obtained with both fluids, it was observed that the pressure drop of ester is on average 7.8 and 7.7 times higher when using ester instead of oil, respectively for the hydraulic and thermohydraulic simulations.

Concerning the thermohydraulic simulations, for the mineral oil, increasing the Reynolds number at the inlet, it was observed a decrease in 28.8 % of the top-oil temperature, 18.3 % of the average-oil temperature and 19.8 % of the average-winding temperature. For the same situation but using ester, the average decrease is of 9.3 % on the top-oil temperature, 5.8 % on the average-oil temperature and 9.5 % on the average-winding temperature.

When increasing the axial channels' width, for mineral oil it is observed an average decrease of 3.7 % in the top-oil temperature, 2.6 % of the average-oil temperature and 2.1 % of the average winding temperature, while for natural ester the average decrease is 1.3 % on top-oil temperature, 1 % on average-oil temperature and 1.1 % on average-winding temperature.

Increasing the radial channels' height is observed that the top-oil temperature does not vary, but the average-oil and average-winding temperatures increase in average 2.3 % and 1.2 %, respectively, using mineral oil, and 0.9 % and 1.2 %, respectively, using natural ester.

It is possible to conclude, that the velocity of the fluid is the parameter that promotes the biggest changes on the overall temperatures, while the axial channel is the geometric parameter whose variation leads to the greatest changes in winding' temperatures.

Comparing both fluids at an inlet temperature of ~43 ºC, the top-oil temperature rise tends to be, in average, 4.1 times higher for mineral oil than for natural ester, while the average-oil temperature rise, and winding temperature are respectively 3.8 times and 21.5 % higher for mineral oil than for natural ester. Therefore, it is concluded that the natural ester is a better coolant than the mineral oil. As a drawback, in terms of flow, the natural ester promotes a considerably high pressure drop comparing to mineral oil, which presents a problem in the power transformer dimensioning.

For the hot-spot temperature, it was concluded that this temperature is influenced by several variables including the flow patterns, therefore more information is needed to have a robust analysis of this value. The HSF generally remained within the recommended range, between 1 and 2. As for the Nusselt number, its increase followed the decrease in the average temperature of the discs, demonstrating that it is higher as the heat is dissipated more efficiently from the discs to the adjacent fluid.

Concerning the machine learning, a new algorithm was developed and trained. The maximum error of the estimator used was 9 % for pressure drop, 10 % for top-oil temperature, 21 % for the average-winding temperature, 10 % for the average-oil temperature, 14 % for the hot-spot temperature, 61.3 % for the HSF and 10 % for the Nusselt number. It is important to highlight that the data generated in the present work is not enough to enable an adequate training of the algorithm but, as the tool is already completely developed, the current lack of robustness can be overcome by simply adding more data to the model.

6 Assessment of the work done

6.1 Objectives Achieved

The study of the variation of geometrical properties in the internal cooling of core type power transformers, for two different fluids, was performed, and the temperature and flow distribution within the winding was determined. The prediction of the thermal results of the transformer internal cooling process was obtained using machine learning.

6.2 Future work

It is suggested as future work, to carry out this study using a wider range of parameters, to have a better understanding about their effect on the internal cooling of a core type power transformer.

Furthermore, is also of extreme importance to obtain more numerical results for other ranges of values, to feed and train the developed algorithm of the machine learning tool, since it was trained for a limited range of values, not allowing a vast prediction of the results.

It is also important to study the effect of natural convection inside the winding.

6.3 Final Assessment

The results obtained in this work, allow to have a good idea on the influence of the design on the thermal performance of a core-type power transformer, however, more results should be obtained to better understand the phenomena. The machine learning tool also showed a great potential on the prediction of the thermal behavior in the winding but need more data to make the tool more accurate.

Personally, this job made me accomplish several milestones. It allowed me to be introduced to the industry and to observe the application of chemical engineering concepts in industrial development. It gave me skills in areas that were not in my domain, such as CFD and Machine Learning, that even though I know I don't come out as an expert, I am able to put into practice in an efficient way. I feel grateful to have had this opportunity and to have developed this work that can pave the way for more exhaustive and applied research on the subject.

7 References

[1] Edison Tech Center, The History of the Transformer, Http://Edisontechcenter.Org/Transformers.Html. (2014). http://edisontechcenter.org/Transformers.html (accessed February 23, 2022).

[2] J.H. Harlow, Electric power transformer engineering, CRC Press, 2004.

[3] EFACEC, EFACEC Web Page - "Quem Somos,", https://www.efacec.pt/quem-somos/ (accessed June 20, 2022).

[4] Sfindor Teszenszkv, History of Transformers, IEEE Power Eng. Rev. (1996) 9–10.

[5] U.S. Department of the interior, Transformers: Basics, Maintenance, and Diagnostics, Denver, Colorado, 2005.

[6] IEC 60076-1 - 2011 - Power Transformers - Part 1 General.

[7] ABB, Liquid-filled power transformers, 2406PL170-W1-En. Ed. 11.2009.

[8] Electrical classroom, Parts of a transformer, Https://Www.Electricalclassroom.Com/Parts-of-a-Transformer/. (2021). https://www.electricalclassroom.com/parts-of-a-transformer/ (accessed February 24, 2022).

[9] Jean Sanchez, Mladen Banovic, Basics of Power Transformers, Transform. Mag. (2014).

[10] Osbert Joel C, Parts of a Power Transformer, Https://Owlcation.Com/Stem/Parts-of-a-Power-Transformer. (2020).

[11] NICORE INDIA, Transformer Core: Essential Things You Must Know, https://nicoreindia.com/transformer-core/ (accessed July 2, 2022).

[12] R.A. Robert M. Del Vecchio, Bertrand Poulin, Pierre T. Feghali, Dilipkumar M. Shah, Transformer Design Principles Third Edition, Taylor & Francis Group, LLC, 2018.

[13] GALCO, Explaining Different Types of Transformers, https://www.galco.com/comp/prod/trnsfmrs.htm (accessed February 25, 2022).

[14] Chris Davis, Core Type vs. Shell Type Distribution Transformers, https://solutions.borderstates.com/core-type-vs-shell-type-distribution-transformers/ (accessed July 2, 2022).

[15] S. Arjuna Rao, G. Girija, Manikandan N, Swaraj Kumar Das, Thermal Performance Of Distribution Transformers, Https://Www.Electricalindia.in/Thermal-Performance-of-Distribution-Transformers/. (2016).

[16] IEC 60076-2 - 2011 - Power Transformers - Part 2 Temperature rise for liquid-immersed transformers.

[17] X. Zhang, M. Daghrah, Z. Wang, Q. Liu, Flow and temperature distributions in a disc type winding-

Part II: Natural cooling modes, Appl. Therm. Eng. 165 (2020). https://doi.org/10.1016/j.applthermaleng.2019.114616.

[18] University of Manchester, IEEE Dielectrics and Electrical Insulation Society, Institute of Electrical and Electronics Engineers, 2017 IEEE 19th International Conference on Dielectric Liquids (ICDL) : 25 June - 29 June, 2017, Manchester, United Kingdom, n.d.

[19] Z. Shen, F. Wang, Z. Wang, J. Li, A critical review of plant-based insulating fluids for transformer: 30-year development, Renew. Sustain. Energy Rev. 141 (2021). https://doi.org/10.1016/j.rser.2021.110783.

[20] T.O. Rouse, Mineral insulating oil in transformers, IEEE Electr. Insul. Mag. 14 (1998) 6–16. https://doi.org/10.1109/57.675572.

[21] 1. Dombek G, Goscinski P, Nadolny Z. Comparison of mineral oil and esters as cooling liquids in high voltage transformer in aspect of environment protection. Energy and Fuels. Published online 2016. doi:10.1051/4

[22] J. Rouabeh, L. M'barki, A. Hammami, I. Jallouli, A. Driss, Studies of different types of insulating oils and their mixtures as an alternative to mineral oil for cooling power transformers, (n.d.). https://doi.org/10.1016/j.heliyon.2019.

[23] P. Rozga, A. Beroual, P. Przybylek, M. Jaroszewski, K. Strzelecki, A review on synthetic ester liquids for transformer applications, Energies. 13 (2020). https://doi.org/10.3390/en13236429.

[24] P. Totzauer, P. Trnka, Different ways to improve natural ester oils, in: Transp. Res. Procedia, Elsevier B.V., 2019: pp. 102–106. https://doi.org/10.1016/j.trpro.2019.07.017.

[25] M.M.M. Salama, D.E.A. Mansour, M. Daghrah, S.M. Abdelkasoud, A.A. Abbas, Thermal performance of transformers filled with environmentally friendly oils under various loading conditions, Int. J. Electr. Power Energy Syst. 118 (2020). https://doi.org/10.1016/j.ijepes.2019.105743.

[26] H.H. Hu, Computational Fluid Dynamics, in: Fluid Mech., Elsevier, 2012: pp. 421–472. https://doi.org/10.1016/B978-0-12-382100-3.10010-1.

[27] X. Zhang, Z. Wang, Q. Liu, P. Jarman, M. Negro, Numerical investigation of oil flow and temperature distributions for ON transformer windings, Appl. Therm. Eng. 130 (2018) 1–9. https://doi.org/10.1016/j.applthermaleng.2017.10.092.

[28] J. Zhang, X. Li, Oil cooling for disk-type transformer windings - Part II: Parametric studies of design parameters, IEEE Trans. Power Deliv. 21 (2006) 1326–1332. https://doi.org/10.1109/TPWRD.2006.871018.

[29] M. Daghrah, X. Zhang, Z. Wang, Q. Liu, P. Jarman, D. Walker, Flow and temperature distributions in a disc type winding-part I: Forced and directed cooling modes, Appl. Therm. Eng. 165 (2020). https://doi.org/10.1016/j.applthermaleng.2019.114653.

[30] M.-I. Farinas, K. Simon KASSI, C. Volat, M. Farinas, K. Kassi, I. Fofana, C. Volat, CFD (Computational Fluid Dynamics) Analysis of Power Transformers Cooling SA2GE: Propulsion for

safe, silent, ecological and efficient URBAN operations-Integration of a de-icing system View project Electrochemical-thermal evaluation of an integrated thermal management system for lithium-ion battery modules with nano-enhanced phase change materials and highly oriented pyrolytic graphite View project CFD Analysis of Power Transformers Cooling, 2016. https://www.researchgate.net/publication/303967332.

[31] L. Raeisian, H. Niazmand, E. Ebrahimnia-Bajestan, P. Werle, Thermal management of a distribution transformer: An optimization study of the cooling system using CFD and response surface methodology, Int. J. Electr. Power Energy Syst. 104 (2019) 443–455. https://doi.org/10.1016/j.ijepes.2018.07.043.

[32] SAS Institute Inc, Machine Learning, (n.d.). https://www.sas.com/pt_pt/insights/analytics/machine-learning.html (accessed June 25, 2022).

[33] IBM, Machine Learning, https://www.ibm.com/cloud/learn/machine-learning (accessed June 25, 2022).

[34] U. Learning, A.N. Network, L. Algorithm, L. Method, H. Belyadi, A. Haghighat, G. Using, Supervised learning AI and Cloud Computing, (2021).

[35] TechTarget, Machine learning, https://www.techtarget.com/searchenterpriseai/definition/machine-learning-ML (accessed June 25, 2022).

[36] Błażej Osiński and Konrad Budek, What is reinforcement learning? The complete guide, (n.d.). https://deepsense.ai/what-is-reinforcement-learning-the-complete-guide/ (accessed June 25, 2022).

[37] T.D. Canonsburg, ANSYS FLUENT User ' s Guide, 2012.

[38] I. ANSYS, 18.4.3 Pressure-Velocity Coupling, https://www.afs.enea.it/project/neptunius/docs/fluent/html/th/node373.htm (accessed June 13, 2022).

[39] Ansys Inc., ANSYS FLUENT Theory Guide, 2020. http://www.afs.enea.it/project/neptunius/docs/fluent/html/th/main_pre.htm (accessed June 13, 2022).

[40] idealsimulations, Courant Number, https://www.idealsimulations.com/resources/courant-number-cfd/ (accessed June 13, 2022).

[41] FISO Technologies Inc., ENERGY Product Catalog.

[42] Yunus A. Çengel, Heat and Mass Transfer A Practical Approach, Third.

[43] G.H. Tang, A.B.M. Rabie, U. Hägg, Indian hedgehog: A mechanotransduction mediator in condylar cartilage, J. Dent. Res. 83 (2004) 434–438. https://doi.org/10.1177/154405910408300516.

[44] Bakshi C. Random Forest Regression. https://levelup.gitconnected.com/random-forest-regression-.

Annex A – Model Validation

In order to confirm the validity of the numerical model to be implemented, a simple exercise concerning the liquid flow and its thermal and hydraulic behavior was performed. The objective was to obtain the minimum number of mesh elements that guarantee the results to be independent from the mesh.

A.1. Geometry

The used geometry, created on ANSYS® SpaceClaim, is represented in the following Figure 35.

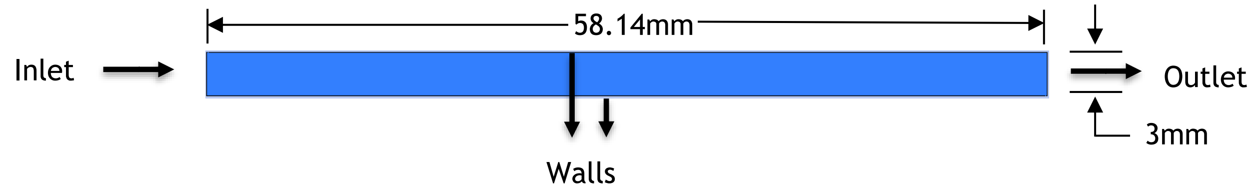

Figure 35 -Geometry used in the independence tests and its boundaries

The design points (i.e. different meshes created) were chosen based on different number of divisions of each of the axes. The first design point consisted of dividing the edges along *x*-axis into 581 parts and the edges along the *y*-axis into 20 parts, and the next ones were developed, increasing those divisions.

A.2. Mesh Independence tests for flow validation

For the mesh independence tests and their flow validation, 6 design points were studied and are represented in Table 19.

Mesh	Design Points	Number of divisions *y* - axis	Number of divisions *x* -axis	Total number of elements
1	0	20	581	11620
2	1	20	1162	23240
3	2	50	581	23050
4	3	100	581	58100
5	4	200	581	116200

Table 19 - Design points used for flow independence tests

For an automatic simulation of the different design points, the number of each axis divisions was defined as an input parameter on ANSYS Meshing, and the parameters were handled on ANSYS Workbench.

The velocity profiles of the fluid were taken, from 5 different lines of the selected geometry. These lines represent 5 different abscissae on the surface domain (Figure 36).

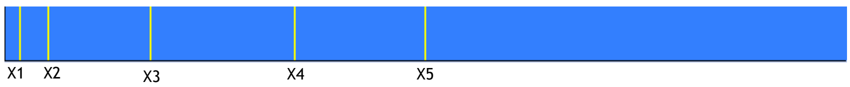

a)

Line	X position / mm
X1	1
X2	3
X3	10
X4	20
X5	29

b)

Figure 36 - a) Geometry chosen and lines used for flow independence tests; b) Lengths ate each line was drawn

The velocity of the liquid was previously defined to guarantee a well-developed flow in the inlet, being used, for that purpose, a parabolic profile to define the velocity, given by Equation 9.

$$v = v_{max}\left(1 - \left(\frac{r^2}{R^2}\right)\right) \tag{9}$$

where v represents the velocity at a radius r, v_{max} the maximum velocity, that is 1.5 times the average velocity, $\bar{v}$, for a 2D rectangular duct, and R is the duct radius, or in this case, half the height. The average velocity is 0.1 m s^{-1}.

As in this case only the oil flow will be analyzed, the simulation ran with the energy disabled, in ANSYS Fluent, and the oil properties were defined as constants, as described in Table 20.

Table 20 - Properties of oil at 60 ºC

Properties	Oil
Density ρ / kg.m^{-3}	846
Dynamic Viscosity μ / Pa.s	0.005

The comparison between the meshes was made by analyzing the velocity profiles at the same position (line X4), as shown in Figure 37. To perform the flow validation, the curves were compared to an analytical solution given by Equation 9.

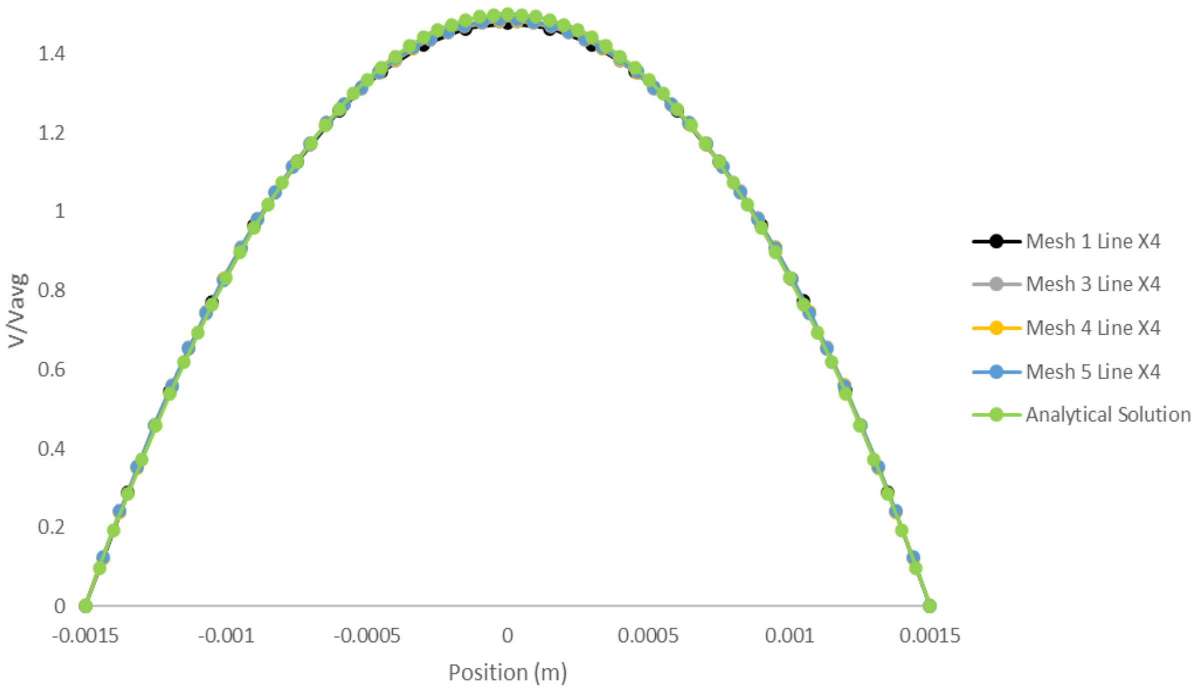

a)

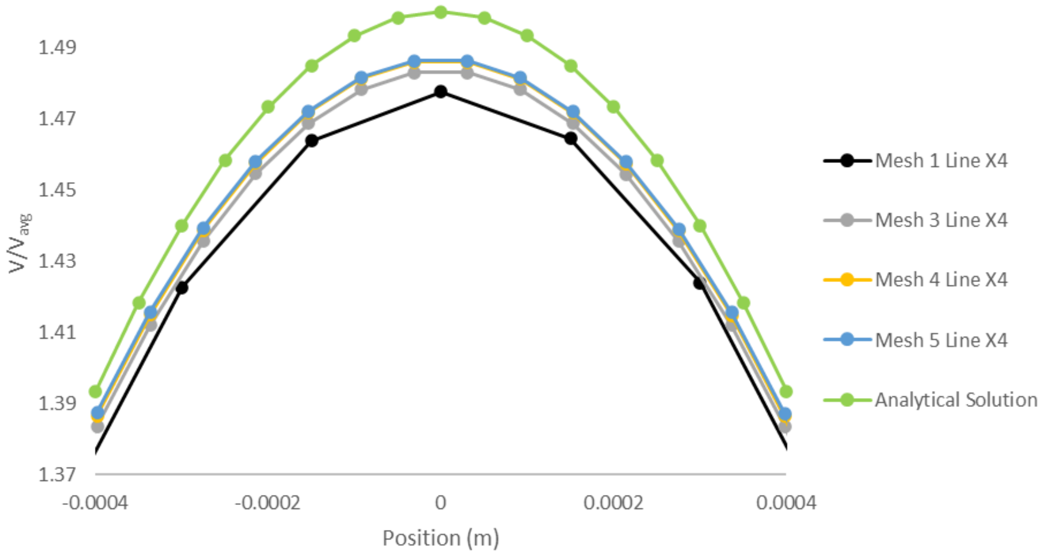

b)

Figure 37 – a, b) Velocity profiles at line X4 for design points 0, 2 ,3, 4 and analytical solution

As shown in Figure 37, in the region where the fluid flow is fully developed, the meshes show results near the analytic value. In this region, when increasing the refinement of the mesh, the meshes 4 and 5 have their velocity profiles almost overlapped (maximum deviation of 0.88%). Therefore, is possible to conclude that the results are independent from the mesh, when using meshes with a refinement at least like mesh 4. This mesh was then chosen to serve as a starting point to proceed with the thermal independence tests and respective thermal validation.

A.3. Mesh independence tests for thermal validation

A.3.1. Thermal mesh independence tests

Independence mesh tests were also performed concerning the thermal behavior of the flowing oil. The simulations were performed in steady state, with the velocity at the inlet defined by a parabolic profile, as in the flow independence tests. In this case, as there is heat transfer, the energy option in ANSYS Fluent was activated and the properties of the oil are defined by a User-Defined Function (Annex B). The boundary conditions were defined as shown in Table 21.

Table 21 - Boundary conditions applied for the thermal verification

Boundary Type	Momentum			Thermal	
	Boundary Condition	U_0 / m s^{-1}	P_0 / Pa	Boundary Condition	T_0 / °C
Inlet	Velocity	0.10	-	Temperature	35
Outlet	Pressure	-	0	-	-
Wall	No Slip	-	-	Temperature	50

Starting with the mesh chosen in the flow independence tests, that have 100 y Divisions and 581 x Divisions several meshes were designed to obtain a mesh capable to provide the less computational effort possible, without compromising the results. Table 22 shows the design points studied.

Table 22 - Meshes used for thermal mesh independence tests

Mesh	Design Points	Number of y Divisions	Number of x Divisions	Number of elements
6	5	100	581	58100
7	6	200	581	116200
8	7	300	581	174300
9	8	400	581	232400
10	9	450	581	261400

The temperature profile in different lines were analyzed. These lines represent 4 different abscissae on the surface domain as shown in Figure 38.

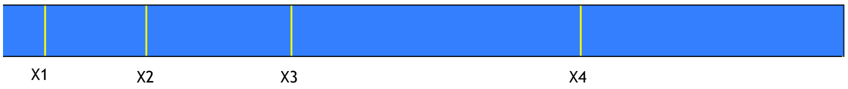

a)

Line	X position / mm
X1	3
X2	10
X3	20
X4	40

b)

Figure 38 - a) Geometry chosen and lines used for thermal independence tests; b) Lengths at each line were drawn

The temperature profiles of the different design points in the same line, X3 (Figure 38b), are shown in Figure 39.

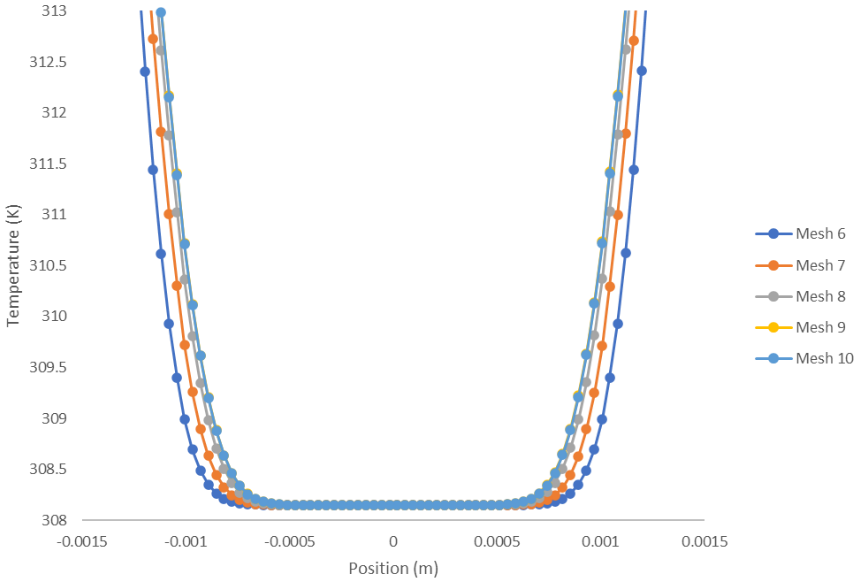

Figure 39 - Temperature profiles for different meshes at X3 line

It is possible to see that the temperature profile of the more refined meshes, tends to overlap, whereas for Meshes 9 and 10, the profile is approximately the same, with a maximum deviation of 0.005%.

Figure 40 shows the heat along on the wall, obtained with different meshes.

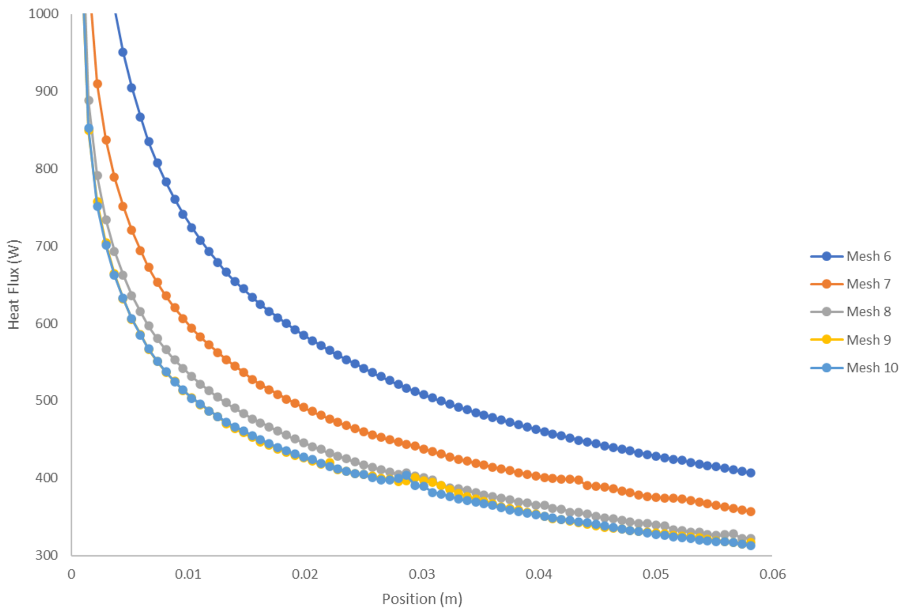

Figure 40 - Heat profile on the walls for each design point

It is possible to see that increasing the number of y-axis divisions, the heat profile on the wall tends to approximate until being almost completely overlapped, with a maximum deviation of 3.37% and an average deviation of 0.56%, and the average Heat value on the wall gets closer as shown on Table 23.

Table 23 - Average heat for each Mesh

Mesh	Average heat (W)	Deviation (%)
6	616.6	
7	519.07	15.8
8	465.33	10.4
9	448.75	3.6
10	447.29	0.3

Analyzing the obtained results, for both the temperature and heat profiles, Mesh 9 was chosen, and the thermal validation was made from it.

A.3.1.1. Thermal Validation

For thermal validation, Mesh 9 was considered, and the simulation conditions remained the same as the ones from the mesh independence tests with the energy equation activated.

The objective of this validation was to compare the value of the wall heat given by ANSYS® Fluent, to the heat transferred to the fluid obtained via analytical solving. The heat transferred to the fluid can be represented by Equation 10.

$$\dot{Q} = \dot{m} * \int_{T_{in}}^{T_{out}} C_p \, dT \tag{10}$$

where $\dot{m}$ is the mass flow rate, C_p is the oil specific heat, T_{in} the average temperature at the inlet and T_{out} the average temperature at the outlet [42]. As the properties of the oil were defined by UDFs, varying with the temperature, the C_p used is an average of the specific heat obtained along all the geometry domain. The values considered for the analytic calculation are presented in Table 24 and they were taken directly from ANSYS Fluent, as outputs of the simulation.

Table 24 - Values used in thermal validation

Parameter	Value
$\dot{m}$ / kg s^{-1}	0.259
T_{out} / K	309.05
T_{in} / K	308.15
C_p / kJ kg^{-1} $°C^{-1}$	1919.8

A deviation of 0.3% between the heat obtained numerically and from equation 2 was achieved, as shown in Table 25, so, the thermal validation was considered completed.

Table 25 -Comparison of heat obtained via simulation and Equation 10

$\dot{Q}_{simulation}$ / W	$\dot{Q}_{equation}$ / W	Deviation
448.75	447.5	0.3 %

Annex B – User defined functions

For reasons of confidentiality , this annex was omitted.

Annex C - Source terms of the discs

Table 26 - Source terms of the discs

Disco	W/Disc	W/m³
1	494	453980
2	495	455376
3	495	455376
4	495	455376
5	495	455376
6	495	455376
7	495	455376
8	495	455376
9	450	413848
10	450	413848
11	450	413848
12	450	413848
13	450	413848
14	450	413848
15	450	413848
16	450	413848
17	447	410984
18	447	410984
19	447	410984
20	447	410984
21	447	410984
22	447	410984
23	447	410984
24	447	410984
25	447	410745
26	447	410745
27	447	410745
28	447	410745
29	447	410745
30	447	410745
31	447	410745
32	447	410745
33	447	411620
34	447	411620
35	447	411620
36	447	411620
37	447	411620
38	447	411620
39	447	411620
40	447	411620
41	447	411620
42	447	411620
43	447	411620
44	447	411620
45	479	441056
46	479	441056
47	479	441056
48	479	441056
49	479	441056
50	479	441056
51	479	441056
52	479	441056
53	479	441056
54	479	441056
55	479	441056
56	479	441056

Annex D - Conditions of mesh independence tests

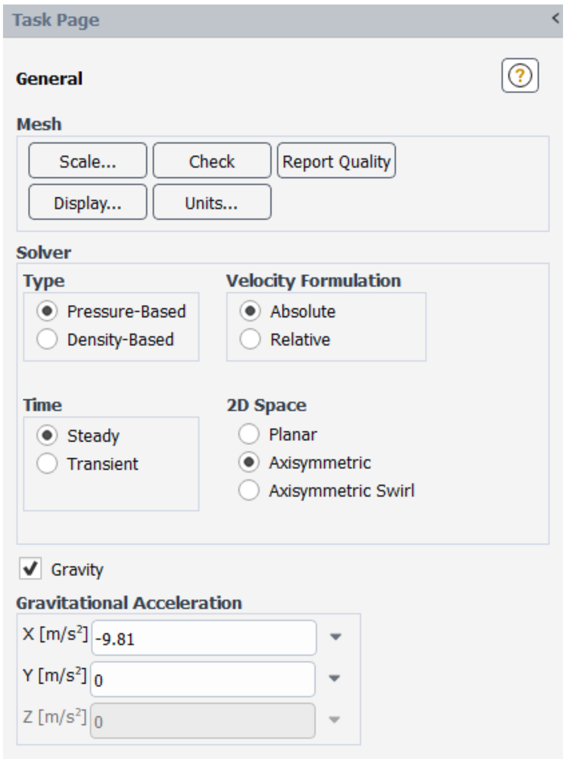

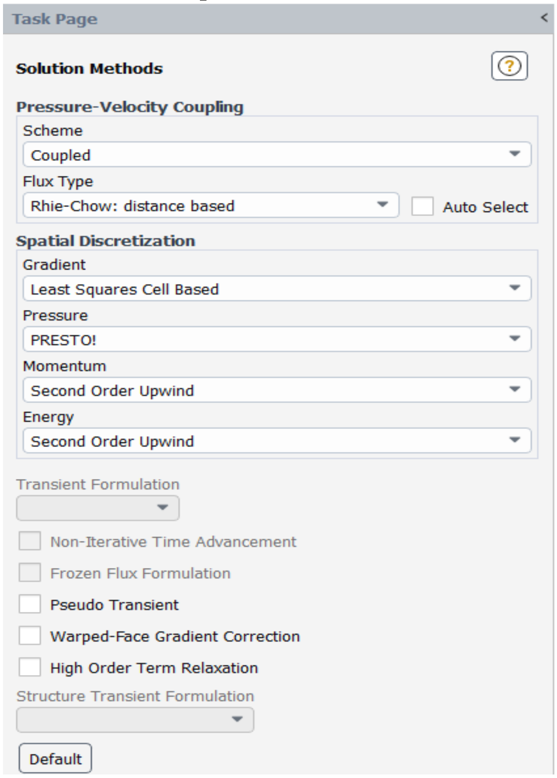

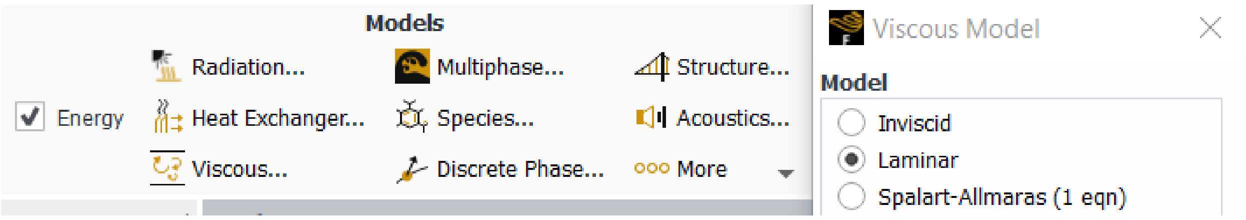

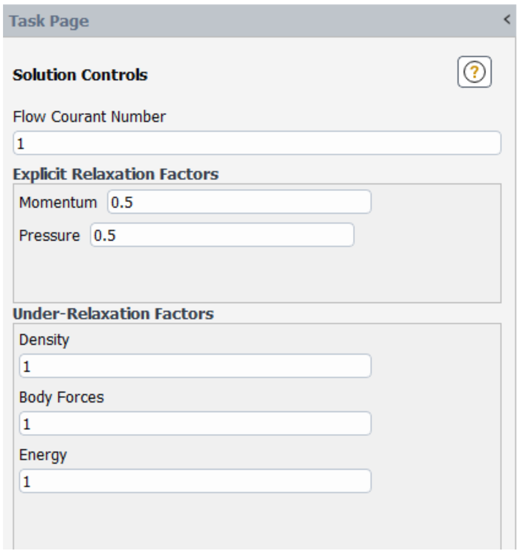

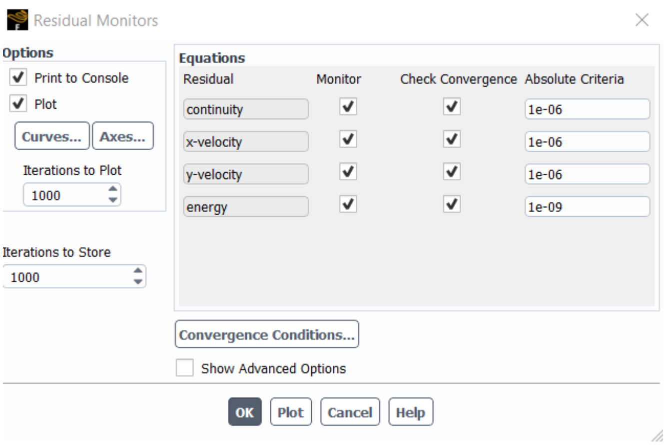

Annex E - Calculation of tangential conductivity for the validation between 2D and 3D geometries

To calculate the tangential conductivity, were used Equation 11 and Equation 12 for parallel resistances considering all discs in the winding as a composition of three materials in parallel, copper, epoxy (resin) and enamel (varnish) as represented in Figure 41 [42].

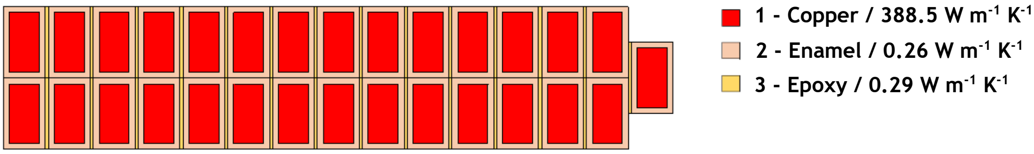

Figure 41 - Parallel Resistances in the winding

$$R_i = \frac{L}{k_i A_i}, i = 1,2,3 \tag{11}$$

$$Q_i = \frac{\Delta T}{R_i}, i = 1,2,3 \tag{12}$$

With R being the resistance, *L* being the length of the material, *k* the thermal conudctivity of the material, *A* the heat transfer area, Q is the heat transferred by a material and ΔT the temperature difference between the hottest and coolest surface of the material.

By linking both equations, and calculating the total heat transferred, appears Equation 13, where the term $\sum_{i=1}^{3} k_i \frac{A_i}{A_T}$ represents the equivalent conductivity and the tangential conductivity of the copper in the discs, used in the simulation, which has the calculated value of 367.35 W $m^{-1}K^{-1}$, and where A_i represents the area of each material and A_T the total area of the geometry.

$$Q_T = \sum_{i=1}^{3} k_i \frac{A_i}{A_T} \frac{A_T}{l} \Delta T \tag{13}$$

Annex F – Process automation

To make the simulation and post-processing more efficient, to run different design points and provide the results automatically, some options were considered, on ANSYS Workbench and its analysis systems and component systems. The procedure is described below.

1. First, it was selected the analysis system, in this case the Fluid Flow (Fluent).

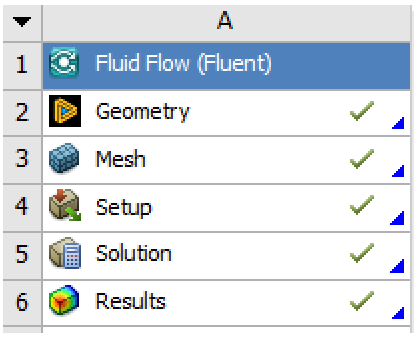

Figure 42 - Fluid Flow (Fluent) Analysis System

2. After the design of the geometry, the mesh was created. For explanatory purpose, the number of divisions of the *x* and *y*-axis of the geometry will be considered as input parameters, selecting the box on the left side of the parameter concerned.

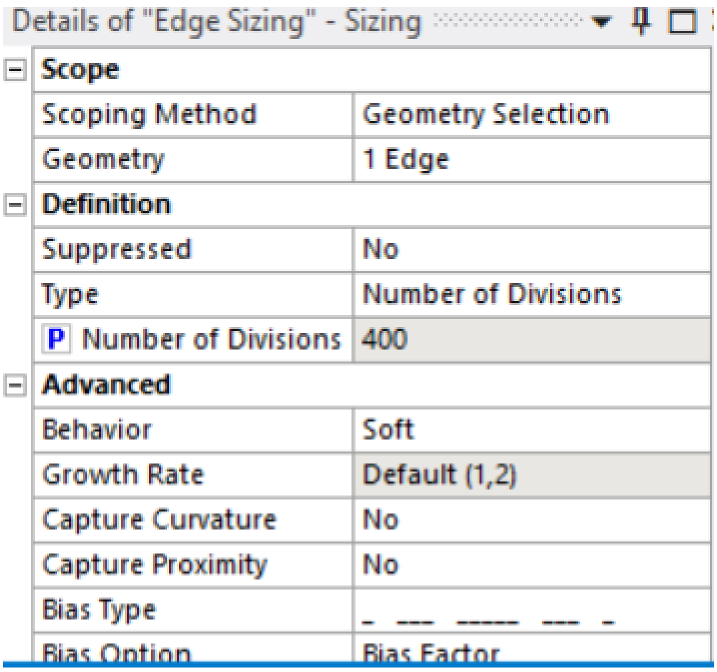

Figure 43 - Edge Sizing options in ANSYS Meshing

3. After selecting the input parameters, automatically, a new "Parameter Set" box will appear in ANSYS Workbench. That box allows to directly handle the different

design points of the project, ordering them in a table, allowing to create new design points and change their values.

	A	B	C	D
1	Name	P3 - Edge Sizing 3 Number of Divisions	P4 - Edge Sizing 4 Number of Divisions	P11 - Edge Sizing 2 Number of Divisions
2	Units			
3	DP 4	581	581	100
4	DP 5	581	581	150
5	DP 6	581	581	200
6	DP 7	581	581	250
7	DP 8	581	581	300
8	DP 9	581	581	350
9	DP 10 (Current)	581	581	400
10	DP 11	581	581	450
*				

Figure 44 – Inputs of Parameter set table

4. Before starting the calculation, it is necessary to define the output parameters, to analyze the results of the simulation. For that, in ANSYS Fluent, is created a new report (as shown in the image below), and after selecting its type, is needed to activate the "Create Output Parameter" option, and it will automatically create the output parameter on the "Parameter Set table". When the "Current" design point is solved, the values of the outputs are presented on the table, and their report is created on the simulation files.

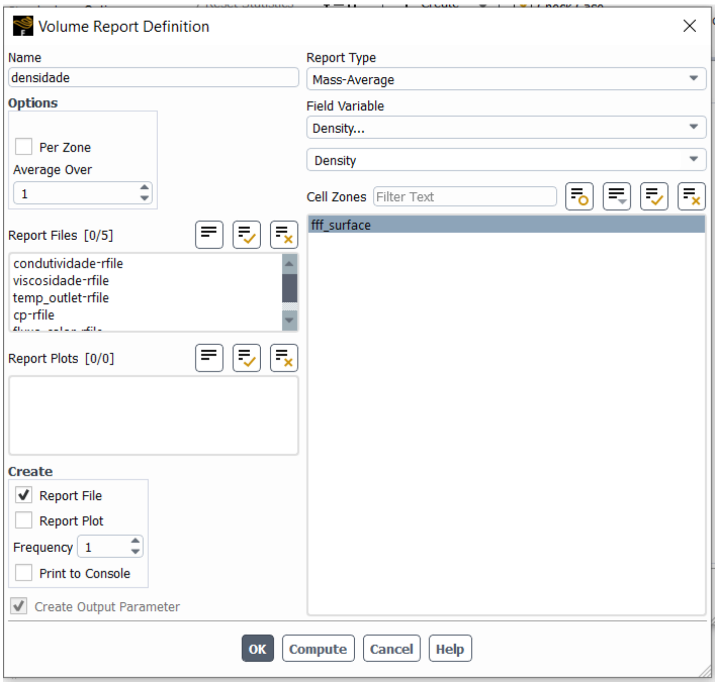

Figure 45 - Definition of a new report

5. In order to simulate all the design points, it is needed to define the design point update process, in the properties of the parameter set. In the option “Retained Design Point” is important to select the “Update full project”, because that will cause each design point to be calculated from scratch, without starting from any already calculated solution of another design point, initializing the calculation.

Properties of Schematic: Parameter Set

	A	B
1	Property	Value
2	Solution Process	
3	Update Option	Run in Foreground
4	Design Point Update Process	
5	Design Point Initiation	From Current
6	Partial Update	None
7	Retain Partial Update	None
8	Retained Design Point	Update full project

Figure 46 - Properties of Parameter Set

6. After doing the last step and clicking on the option “Update all design points”, all the calculations will be made, one in a turn, the results are automatically presented on parameter set table in ANSYS Workbench.

F	G	H	I	J	K
P5 - fluxo_calor-op	P6 - cp-op	P8 - viscosidade-op	P9 - condutividade-op	P10 - densidade	P13 - temp_outlet-op
W	J kg^-1 K^-1	Pa s	W m^-1 K^-1	kg m^-3	K
616,6	1920,6	0,0096799	0,13196	861,32	309,38
567,55	1920,3	0,0096989	0,13197	861,22	309,28
519,07	1920,1	0,0097178	0,13197	861,1	309,19
483,39	1919,9	0,0097316	0,13197	860,99	309,12
465,33	1919,9	0,0097387	0,13198	860,92	309,08
455,55	1919,8	0,0097428	0,13198	860,88	309,06
448,75	1919,8	0,0097453	0,13198	860,86	309,05
447,29	1919,8	0,0097465	0,13198	860,85	309,04

Figure 47 - Outputs of the Parameter Set Table

7. If it is intended to analyze any type of chart, contour plots, or vector plots, it is also possible to export them automatically, while doing the update to all design points. For that, in ANSYS CFD-Post, it should be created and then selected all the reports wanted for further analysis.

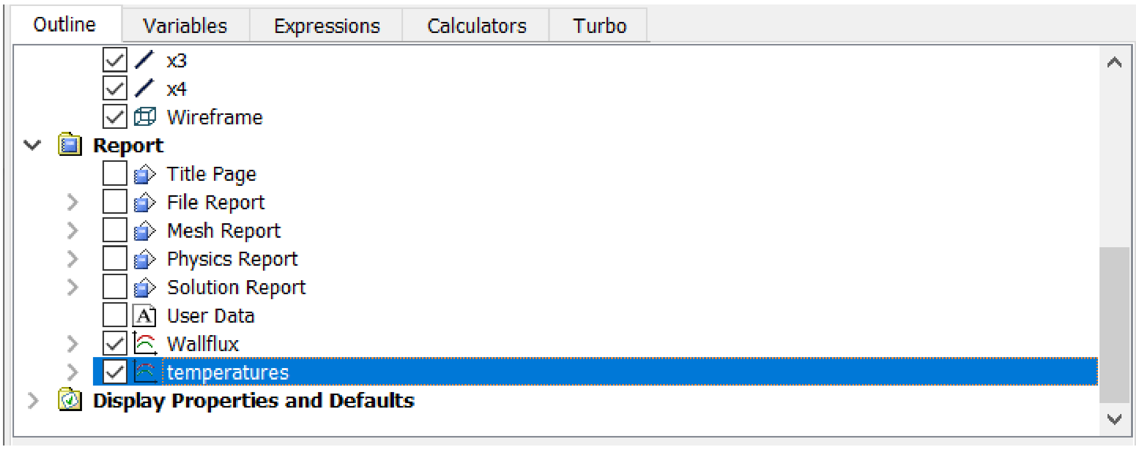

Figure 48 - Reports selection in ANSYS CFD-Post

8. To enable the automatic saving of the reports, it is necessary to open the "Properties" of CFD-Post and select the option "Publish Report". That will create a directory, on the top folder of the simulation case, with the name "report files", where for each design points, the reports selected on CFD-Post will be written.

Properties of Schematic A6: Results

	A	B
1	Property	Value
2	⊟ General	
3	Always Include in Design Point Update	☑
4	Component ID	Results
5	Directory Name	FFF
6	⊟ Notes	
7	Notes	
8	⊟ Used Licenses	
9	Last Update Used Licenses	cfd_base cfd_preppost
10	⊟ Update Options	
11	Clear State	☐
12	Load Report	None
13	Publish Report	☑
14	Report Output Filename	Report
15	Report Location	

Figure 49 - Properties of Results

Annex G -Results

Table 27 - Results of hydraulic simulations for mineral oil

Radial channel / mm	Axial channel / mm	Re	ΔP / Pa
4	6	79	53.39
4	6	247	166.68
4	6	643	645.8
4	7	79	45.21
4	7	247	145.16
4	7	643	600.24
4	8	79	40.32
4	8	247	132.75
4	8	643	579.74
5	6	79	50.55
5	6	247	160.52
5	6	643	630.34
5	7	79	41.38
5	7	247	136.21
5	7	643	579.58
5	8	79	35.59
5	8	247	121.17
5	8	643	554.39
6	6	79	49.37
6	6	247	158.43
6	6	643	624.52
6	7	79	39.64
6	7	247	132.48
6	7	643	571.56
6	8	79	33.33
6	8	247	115.98
6	8	643	544.97

Table 28 - Results of hydraulic simulations for natural ester

Radial channel / mm	Axial channel / mm	Re	DP / Pa
4	6	79	643.58
4	6	247	2203.91
4	6	643	8445.42
4	7	79	544.35
4	7	247	1919.81
4	7	643	7847.24
4	8	79	485.04
4	8	247	1755.94
4	8	643	7577.39
5	6	79	608.78
5	6	247	2122.74
5	6	643	8242.93
5	7	79	497.7
5	7	247	1801.7
5	7	643	7576.09
5	8	79	427.39
5	8	247	1603.1
5	8	643	7244.68
6	6	79	594.18
6	6	247	2095.16
6	6	643	8166.88
6	7	79	476.3
6	7	247	1752.54
6	7	643	7401.06
6	8	79	399.71
6	8	247	1534.63
6	8	643	7121.15

Table 29 - Results of thermohydraulic simulations for mineral oil

Radial channel / mm	Axial channel / mm	Re	ΔP / Pa	Top-oil / °C	Av.fluid / °C	Av.winding / °C	Hot-Spot / °C	HSF	Nusselt
4	6	79	73.2	85.7	67.0	82.5	100.9	0.84	4.36
4	6	247	204.4	59.5	52.2	64.1	72.2	1.01	5.83
4	6	643	777.1	49.5	47.1	55.9	63.3	1.46	6.98
5	6	79	67.7	85.7	67.2	82.4	101.2	0.87	4.07
5	6	247	200.4	59.5	52.6	65.1	72.8	0.98	5.64
5	6	643	757.7	49.5	47.2	56.5	65.6	1.59	6.46
6	6	79	65.7	85.7	72.3	83.8	102.2	0.86	3.73
6	6	247	201.5	59.5	54.8	66.4	78.8	1.29	4.93
6	6	643	750.2	49.5	48.0	57.0	66.0	1.57	5.97
4	7	79	68.7	79.9	64.1	80.0	102.2	1.21	4.20
4	7	247	177.1	57.2	50.8	62.4	69.9	1.05	5.57
4	7	643	702.6	48.7	46.6	55.3	63.4	1.59	6.56
5	7	79	64.8	79.9	63.7	79.6	97.3	0.97	3.938
5	7	247	168.6	57.2	51.1	63.3	70.5	1.02	5.17
5	7	643	673.1	48.7	46.9	56.1	68.4	1.96	6.10
6	7	79	61.7	79.9	68.5	81.0	97.2	0.89	3.63
6	7	247	167.8	57.2	53.2	64.3	71.8	1.04	4.79
6	7	643	660.7	48.7	47.7	56.6	70.5	2.07	5.67
4	8	79	58.8	75.5	61.4	77.0	93.1	1.00	4.05
4	8	247	161.1	55.5	49.9	61.3	68.1	1.06	5.28
4	8	643	662.2	48.0	46.4	54.9	63.0	1.62	6.15
5	8	79	53.0	75.5	61.4	77.6	92.4	0.93	3.77
5	8	247	148.4	55.5	50.1	62.1	68.8	1.05	4.94
5	8	643	623.2	48.0	46.6	55.7	66.5	1.85	5.75
6	8	79	51.7	75.5	65.4	78.5	95.3	1.04	3.54
6	8	247	145.3	55.5	52.0	63.0	70.7	1.12	4.60
6	8	643	604.8	48.0	47.3	56.2	68.8	1.98	5.36

Table 30 - Results of thermohydraulic simulations for natural ester

Radial channel / mm	Axial channel / mm	Re	ΔP / Pa	Top-oil / ºC	Av.fluid / ºC	Av.winding / ºC	Hot-Spot / ºC	HSF	Nusselt
4	6	79	862.8	54.6	49.8	60.3	66.2	1.03	5.35
4	6	247	3125.9	47.1	45.6	53.1	56.4	1.18	6.28
4	6	643	10672.8	44.8	44.3	50.0	53.3	1.43	6.80
5	6	79	820.3	54.6	50.4	61.6	70.5	1.26	4.89
5	6	247	2991.7	47.1	45.8	53.6	58.0	1.29	5.81
5	6	643	10377.0	44.8	44.4	50.4	54.3	1.50	6.32
6	6	79	804.7	54.6	52.0	63.2	76.1	1.51	4.45
6	6	247	2940.1	47.1	46.3	54.2	60.1	1.45	5.34
6	6	643	10277.0	44.8	44.5	50.6	54.8	1.52	5.87
4	7	79	735.5	53.0	48.7	58.9	64.3	1.06	5.09
4	7	247	2689.2	46.6	45.2	52.6	55.5	1.17	5.87
4	7	643	9573.8	44.6	44.2	49.8	53.4	1.50	6.33
5	7	79	676.4	53.0	49.1	59.9	65.7	1.09	4.70
5	7	247	2501.2	46.6	45.4	53.1	56.3	1.20	5.49
5	7	643	9124.0	44.6	44.2	50.2	55.2	1.69	5.92
6	7	79	650.2	53.0	50.5	61.1	69.6	1.28	4.20
6	7	247	2418.4	46.6	45.8	53.5	57.1	1.23	5.1
6	7	643	8942.4	44.6	44.4	50.6	56.4	1.79	5.52
4	8	79	657.0	51.9	48.0	58.0	62.9	1.06	4.80
4	8	247	2430.1	46.2	45.0	52.3	55.0	1.18	5.49
4	8	643	8964.8	44.4	44.1	49.7	53.8	1.61	5.90
5	8	79	582.5	51.9	48.2	58.8	64.0	1.08	4.48
5	8	247	2190.8	46.2	45.1	52.7	55.8	1.20	5.16
5	8	643	8373.5	44.4	44.2	50.2	56.3	1.90	5.55
6	8	79	547.3	51.9	49.5	59.8	65.5	1.11	4.03
6	8	247	2078.0	46.2	45.5	53.2	56.6	1.24	4.83
6	8	643	8132.0	44.4	44.4	50.6	58.0	2.03	5.19

Annex H – Machine learning tool’s code

```
#libraries import
import pandas as pd
import numpy as np
import matplotlib.pyplot as plt

import seaborn as sns
#import quickda

import sklearn

from sklearn import svm
from sklearn import ensemble
from sklearn.model_selection import cross_validate

#data import
hidoil=pd.read_excel (r'C:\Users\10345\OneDrive - EFACEC Power Solutions, SGPS, SA\Ambiente de Trabalho\RESULTADOS ML.xlsx',sheet_name='Hidraulica oleo')
hidester=pd.read_excel (r'C:\Users\10345\OneDrive - EFACEC Power Solutions, SGPS, SA\Ambiente de Trabalho\RESULTADOS ML.xlsx',sheet_name='Hidraulica ester')
hid=pd.read_excel (r'C:\Users\10345\OneDrive - EFACEC Power Solutions, SGPS, SA\Ambiente de Trabalho\RESULTADOS ML.xlsx',sheet_name='Hidraulica')

termooil=pd.read_excel (r'C:\Users\10345\OneDrive - EFACEC Power Solutions, SGPS, SA\Ambiente de Trabalho\RESULTADOS ML.xlsx',sheet_name='Termohidraulica oleo')
termoester=pd.read_excel (r'C:\Users\10345\OneDrive - EFACEC Power Solutions, SGPS, SA\Ambiente de Trabalho\RESULTADOS ML.xlsx',sheet_name='Termohidraulica ester')
termo=pd.read_excel (r'C:\Users\10345\OneDrive - EFACEC Power Solutions, SGPS, SA\Ambiente de Trabalho\RESULTADOS ML.xlsx',sheet_name='Termohidraulica')

#variables naming
xhidoil=hidoil[["radial","axial","Re","Fluid"]]
xhidoil=pd.get_dummies(xhidoil,columns=["Fluid"],drop_first=True)
yhidoil=hidoil[["Pressao"]]

xhidester=hidester[["radial","axial","Re","Fluid"]]
xhidester=pd.get_dummies(xhidester,columns=["Fluid"],drop_first=True)
yhidester=hidester[["Pressao"]]

xhid=hid[["radial","axial","Re","Fluid"]]
xhid=pd.get_dummies(xhid,columns=["Fluid"],drop_first=True)
yhid=hid[["Pressao"]]
```

```
xtermooil=termooil[["radial","axial","Re","Fluid"]]
xtermooil=pd.get_dummies(xtermooil,columns=["Fluid"],drop_first=True)
ytermooil=termooil[["Pressao", "Top-oil","Oleo-medio", "Cobre-medio", "Hot-Spot",
"HSF", "Media do oleo","Nusselt"]]

xtermoester=termoester[["radial","axial","Re","Fluid"]]
xtermoester=pd.get_dummies(xtermoester,columns=["Fluid"],drop_first=True)
ytermoester=termoester[["Pressao", "Top-oil","Oleo-medio", "Cobre-medio", "Hot-Spot",
"HSF", "Media do oleo","Nusselt"]]

xtermo=termo[["radial","axial","Re","Fluid"]]
xtermo=pd.get_dummies(xtermo,columns=["Fluid"],drop_first=True)
ytermo=termo[["Pressao", "Top-oil","Oleo-medio", "Cobre-medio", "Hot-Spot", "HSF",
"Media do oleo","Nusselt"]]

#Random Forest regressor
from sklearn.ensemble import RandomForestRegressor

rf=RandomForestRegressor(n_estimators=100, random_state=42)

rf.fit(xtermo, ytermo)


#Random Forest regressor for HSF
from sklearn.ensemble import RandomForestRegressor
from sklearn.svm import SVR
import numpy as np

rf=RandomForestRegressor(n_estimators=100, random_state=42)

rf.fit(xtermo, ytermo)

rfhsf = RandomForestRegressor(n_estimators=800, random_state=42)

rfhsf.fit(xtermo,ytermo[['HSF']])

#Simulator
from tkinter import*
root=Tk()
root.title("Simulator")

e1 = Entry(root, borderwidth=5)
e2 = Entry(root, borderwidth=5)
e3 = Entry(root, borderwidth=5)
e4 = Entry(root, borderwidth=5)

e1.grid(row=0,column=1)
e2.grid(row=1,column=1)
e3.grid(row=2,column=1)
e4.grid(row=3,column=1)
```

```
e1.get()
e2.get()
e3.get()
e4.get()

Label1 = Label(root, text="Radial channel / mm")
Label2 = Label(root, text='Axial channel / mm')
Label3 = Label(root, text='Reynolds number')
Label4 = Label(root, text='Fluid (0=ester, 1=oil)')

Label1.grid(row=0,column=0)
Label2.grid(row=1, column=0)
Label3.grid(row=2,column=0)
Label4.grid(row=3,column=0)

def myClick():
    list1 = [e1.get(),e2.get(),e3.get(),e4.get()]
    Y_pred=rf.predict(np.array(list1).reshape(-4,4))
    Y_out=rfhsf.predict(np.array(list1).reshape(-4,4))
    pres_out=round(Y_pred[0,0],2)
    topOil_out=round(Y_pred[0,1]-273.15,2)
    avOil_out=round(Y_pred[0,2]-273.15,2)
    avCop_out=round(Y_pred[0,3]-273.15,2)
    hotspot_out=round(Y_pred[0,4]-273.15,2)
    nusselt_out=round(Y_pred[0,7],2)
    HSF_out=round(Y_out[0],2)

    presure = Label(root,text = "Pressure Loss / Pa= ")
    presure_pred= Label(root,text=pres_out)

    topoil = Label(root, text="Top-oil / ºC= ")
    topoil_pred= Label(root,text=topOil_out)

    avoil = Label(root, text="Average-oil / ºC= ")
    avoil_pred= Label(root,text=avOil_out)

    avcop = Label(root, text="Average-winding / ºC= ")
    avcop_pred= Label(root,text=avCop_out)

    hotspot = Label(root, text="Hot-Spot / ºC= ")
    hotspot_pred = Label(root, text=hotspot_out)

    HSF= Label(root, text="HSF= ")
    HSF_pred=Label(root, text=HSF_out)

    nuss= Label(root, text="Nusselt number= ")
    nuss_pred= Label(root,text=nusselt_out)
    #Output1 = Label(root,text = e1.get())
    #Output2 = Label(root,text = e2.get())
    #Output3 = Label(root,text = e3.get())
    #Output4 = Label(root,text = e4.get())
```

```
    presure.grid(row=0, column=3)
    presure_pred.grid(row=0, column=4)

    topoil.grid(row=1, column=3)
    topoil_pred.grid(row=1, column=4)

    avoil.grid(row=2, column=3)
    avoil_pred.grid(row=2, column=4)

    avcop.grid(row=3, column=3)
    avcop_pred.grid(row=3, column=4)

    hotspot.grid(row=4, column=3)
    hotspot_pred.grid(row=4, column=4)

    HSF.grid(row=5, column=3)
    HSF_pred.grid(row=5, column=4)

    nuss.grid(row=6, column=3)
    nuss_pred.grid(row=6, column=4)
    return

myButton = Button(root, text="Calculate", command=myClick)
myButton.grid(row=4,column=0)

root.mainloop()
```